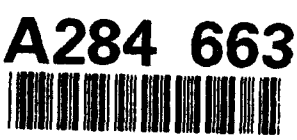

PL-TR-94-2161

NEW APPLICATIONS OF THE PHILLIPS LABORATORY THEORETICAL IONOSPHERIC MODEL AND STUDIES OF NEUTRAL DENSITY WAVES

Matthew W. Fox, Xiaoqing Pi and Jeffrey M. Forbes

Boston University Center for Space Physics

725 Commonwealth Avenue

Boston, Massachusetts 02215

Scientific Report No. 1

April 1994

PHILLIPS LABORATORY
Directorate of Geophysics
AIR FORCE MATERIEL COMMAND
HANSCOM AFB, MA 01731-3010

"This technical report has been reviewed and is approved for publication"

(Signature)
FRANK A. MARCOS
Contract Manager

(Signature)
DAVID N. ANDERSON
Branch Chief

(Signature)
WILLIAM K. VICKERY
Division Director

This report has been reviewed by the ESC Public Affairs Office (PA) and is releasable to the National Technical Information Service (NTIS).

Qualified requestors may obtain additional copies from the Defense Technical Information Center (DTIC). All others should apply to the National Technical Information Service (NTIS).

If your address has changed, if you wish to be removed from the mailing list, or if the addressee is no longer employed by your organization, please notify PL/IM , 29 Randolph Road, Hanscom Road, Hanscom AFB, MA 01731-3010. This will assist us in maintaining a current mailing list.

Do not return copies of this report unless contractual obligations or notices on a specific document requires that be returned.

REPORT DOCUMENTATION PAGE

Form Approved
OMB No. 0704-0188

1. AGENCY USE ONLY (Leave blank)	2. REPORT DATE	3. REPORT TYPE AND DATES COVERED
	April 1994	Scientific No. 1

4. TITLE AND SUBTITLE
New Applications of the Phillips Laboratory Theoretical Ionospheric Model and Studies of Neutral Density Waves

5. FUNDING NUMBERS
PE 63707F
PR 4026 TA GL WU MA

Contract F19628-93-K-0012

6. AUTHOR(S)
Matthew W. Fox
Xiaoqing Pi
Jeffrey M. Forbes*

7. PERFORMING ORGANIZATION NAME(S) AND ADDRESS(ES)
Boston University
Center for Space Physics
725 Commonwealth Avenue
Boston, MA 02215

8. PERFORMING ORGANIZATION REPORT NUMBER

9. SPONSORING/MONITORING AGENCY NAME(S) AND ADDRESS(ES)
Phillips Laboratory
29 Randolph Road
Hanscom AFB, MA 01731-3010

Contract Manager: Frank Marcos/GPIM

10. SPONSORING/MONITORING AGENCY REPORT NUMBER
PL-TR-94-2161

11. SUPPLEMENTARY NOTES
* University of Colorado, Dept. of Aerospace Engr Sciences, Boulder, CO 80303-0429

12a. DISTRIBUTION/AVAILABILITY STATEMENT
Approved for public release;
distribution unlimited

12b. DISTRIBUTION CODE

13. ABSTRACT *(Maximum 200 words)*

Firstly, a series of new applications for the PHILLIPS Laboratory ionospheric model have been developed;a version has been prepared that allows restarts from specified background conditions, and runs have been made of both impulsive (e.g., storm onset) and periodic (e.g., atmospheric wave) perturbed conditions. Comparison studies are the subject of ongoing work. Secondly, tests of a new plasmaspheric model have been conducted with a view to merging it with the PL model in a new version of PRISM. Thirdly, the PL model has been applied to a study of the low latitude ionosphere involving comparisions of the observed longitudinal and seasonal morphology of irregularities. Next, a version of the model has been prepared that permits a study of the effects of substorms through modifications of the vertical drift and neutral wind fields. Case studies at different longitudes identified increases in TEC with substorm expansion phases and decreases with substorm subsidence. Finally, SETA measurements of neutral density variations have been utilized in a study of both small-scale (up to 2500 km) and larger scale wave phenomena, including descriptions of diurnal and magnetic activity dependencies.

14. SUBJECT TERMS		15. NUMBER OF PAGES
Theoretical Modeling Applications Modeling	Neutral density waves	68
		16. PRICE CODE

17. SECURITY CLASSIFICATION OF REPORT	18. SECURITY CLASSIFICATION OF THIS PAGE	19. SECURITY CLASSIFICATION OF ABSTRACT	20. LIMITATION OF ABSTRACT
Unclassified	Unclassified	Unclassified	SAR

TABLE OF CONTENTS

1. INTRODUCTION 1

2. MODELING PERTURBED IONOSPHERIC CONDITIONS 1

2.1 Storm Onset 2

2.1.1 Low Latitude Storms 3

2.1.2 Middle Latitude Storms 6

2.2 Ionospheric Waves 8

3. EXTENSIONS TO THE PRISM MODEL 10

3.1 Description of the Bailey Model 11

3.2 Model Validation and Comparisons 11

4. EQUATORIAL IONOSPHERE STUDY 14

4.1 Spread-F Morphology 14

4.2 Modeling Asymmetries 15

4.3 The Effects of Magnetic Activity 16

5. SUBSTORM MODELING STUDY 17

5.1 Introduction 18

5.2 The Observed Events at Two Longitudes 18

5.3 Modeling TEC Disturbances 19

5.4 Discussion and Conclusions 22

6. NEUTRAL DENSITY WAVES 23

6.1 Small-scale waves 23

6.1.1 Spectral Analysis 24

6.1.2 Periodogram Averaging 25

6.1.3 Wavelength Contribution to Signal Energy 26

6.2 Large-scale waves 27

7. REFERENCES 30

Illustrations

Figure 1. Diurnal variations of TEC for US Sector, Equinox, solar maximum conditions at six selected dip latitudes. The solid line denotes background variations. The dotted and dashed lines respectively show the variations in TEC after a switch to active conditions at 00LT for the subsequent two days. the mean values of each of TEC, Nmax and τ in the Hamilton, MA region.

Figure 2. The same as Figure 1, but onset time is 06LT.

Figure 3. The same as Figure 1, but onset time is 12LT.

Figure 4. The same as Figure 1, but onset time is 18LT.

Figure 5. A comparison of observed and predicted storm-time variations in TEC at Hamilton, MA, for a storm on March 12, 1971. The solid line shows the deviation expressed as a percentage from the 31-day running mean in the data, from the previous day, through to four days past storm onset. The vertical dotted lines denote local midnight. The dotted, dashed and dot-dashed curves show the modeled variations in MIDLAT, at dip latitudes of 40, 45 and 50 degrees respectively.

Figure 6. As in Figure 5, but for a storm on January 23, 1979.

Figure 7. Observed variations in foF2 from several low latitude stations, in late August 1979, showing evidence for two-day periodicity.

Figure 8. The variations in foF2, appropriate to the conditions in Figure 7, obtained by LOWLAT, and by adjusting the vertical drift pattern from the climatological average. Generally good agreement is obtained. at solar minimum and solar maximum.

Figure 9. An example of the variations in foF2 when a two-day wave perturbation is introduced into the background vertical drift pattern used to derive the mean variations in Figure 7. Four panels show the variations at four selected latitudes. Vertical solid and dotted lines in each panel denote local midnight and noon. The solid line is the background (pre-event) variation and is repeated for several days to facilitate comparisons. The dotted line shows the variation in foF2 under the additional influence of a wave of amplitude $3ms^{-1}$ commenced at 21LT. Two-day variations are evident at 16 and 20 degrees.

Figure 10. An example of the variations in 16LT values of foF2 at three selected latitudes under the influence of a 16-day wave (of amplitude 50%) on the ambient vertical drift pattern. The wave-like variations in foF2 are made apparent compared to the background values, seen as a straight line.

Figure 11. A comparison of results of the Baily model and the GTIM. Solid line = Bailey model output; Dotted line = GTIM output, including direct photoionization only; Dashed line = GTIM output, including direct and secondary photoionization; Dot-Dashed line = GTIM output, including direct photoionization and photodissociation. It can be seen that the secondary and photodissociative terms are very similar in magnitude.

Figure 12. A comparison of results of the Baily model and the GTIM. Solid line = Bailey model output; Dotted line = GTIM output, including direct photoionization only; Dashed line = GTIM output, including direct photoionization and photodissociation; Dot-Dashed line = GTIM output, including direct and secondary photoionization and photodissociation. The overall agreement between the sum of terms in GTIM and the Bailey code is reasonable.

Figure 13. A summary of the characteristics of the Asian sector, solar maximum ionosphere, as derived in GTIM. Contours of electron density at 21LT are shown for six months to demonstrate the seasonal variations. The level of symmetry is contrasted to spread-F morphology in the text.

Figure 14. As in Figure 13, but for the Indian sector.

Figure 15. As in Figure 13, but for the Peruvian sector.

Figure 16. As in Figure 13, but for the Brazilian (Natal) sector.

Figure 17. Figure 18 from Aarons (1993), as a convenient summary of the occurrence of evening spread-F as a function of longitude and season.

Figure 18. A revision of the Natal sector runs of Figure 16, but using a hardwired higher declination value in GTIM than is predicted by the simple magnetic field model within GTIM. Better agreement is obtained here with spread-F occurrence rates.

Figure 19. As in Figure 13, but demonstrating the results obtained from GTIM in the presence of disturbed vertical drift patterns, as described in the text.

Figure 20. TEC disturbance events on July 29 and 30, 1982, at four middle and lower latitude sites in the longitudes of near 75°W (Hamilton, KSC, and Ramey) and 7°E (Florence, Italy) are plotted with auroral electrojet (AU/AL, top) and ring current (Dst, bottom) indices. One TEC unit in the figure represents 10^{16} el m^{-2}. Shaded areas indicate $\pm$ one standard deviation of 31 day TEC average values centered at the day of July 30. Filled circles indicate the local noon at the four sites. Magnetic daily index (Ap) values are also shown above the top panel.

Figure 21. A TEC disturbance event on January 31, 1981, shown in the same format as Figure 20.

Figure 22. Ionospheric model results for electrodynamical candidate processes operating during substorms. Panel (a) and (f) show the substorm activity context specified by auroral AU/AL and ring current Dst indices, respectively. Simulation results are given for the event on July 30, 1982, at one site in the European sector (Forence, (b)) and two sites in the American sector (KSC (c) and Ramey (d)), together with observations and modeling of TEC mean behavior. The required electric field perturbations (positive for eastward) for the three sites are also shown in (e). The vertical dotted lines separate periods of expanding and subsided substorm activities. The filled circles give local noon at each site.

Figure 23. An averaged periodogram of neutral density waves observed in the SETA 1983 data. The solid/dashed line corresponds to geomegnetically quiet/active times. The enhancement of longer-wavelength wave activity in active periods is evident.

Figure 24. An averaged periodogram of neutral density waves observed in the SETA 1983 data. The solid/dashed line corresponds to daytime/nighttime values. The enhancement of shorter-wavelength wave activity at night is evident.

Figure 25. Averaged daytime low-latitude density values derived from SETA density measurements in late July 1983. Periodicities of 8-12 hours are apparent in this figure.

1. INTRODUCTION

The Phillips Laboratory Global Theoretical Ionospheric Model, or GTIM, (Anderson, 1973a) has been used over a number of years and for a variety of applications. The model itself determines solutions for O^+ densities along magnetic field lines in the presence of a specified thermosphere and solar input. Because this is simply an ionospheric solution to the designated input conditions, it is a model well-suited to investigative, or diagnostic, modeling studies whereby certain inputs are changed and the ionospheric response is monitored. Further, as the model has undergone significant use and validation since its inception, the credibility in the model is there for the development of various empirical summaries of the model output, such as SLIM (Anderson et al., 1987) and most recently PRISM (Daniell et al., 1994), and for using the model to establish interrelationships between ionospheric and other observable parmeters (e.g., Fox et al., 1994). Further, the model is undergoing continual active validation through the auspices of collaborative working groups such as PRIMO and PRIME.

In this report, several new applications for the GTIM are presented with the broad goal of extending the model to new regimes and thereby increase its scope.

2. MODELING PERTURBED IONOSPHERIC CONDITIONS

Existing applications of the GTIM include ionospheric climatology studies (e.g., Anderson, 1973b; Daniell et al., 1994; Klobuchar et al., 1991) diagnostic modeling studies of selected phenomena (e.g., Pi et al., 1993), and case studies of particular periods of interest (e.g., Preble et al., 1994). It has thus been established as a useful and reliable model of the F-region ionosphere. On the other hand, it could be argued that it is sensitive to externally input conditions, such as the composition, neutral wind and vertical drift fields, given that the model derives an ionospheric solution in the presence of the specified conditions. However, this does not exclude either climatological or diagnostic

modeling studies as these quantities are fairly well-known, on average. And for case studies, thermospheric or other inputs may well be available (e.g., Anderson et al., 1992; Preble et al., 1994).

One application of this model that has not previously been explored is the study of an ionosphere in conditions that may change from one day to another. In particular, we wish to first allow the model ionosphere to converge to background conditions, then to follow the model from this point under different, perturbed conditions. An extension to the GTIM has been prepared at Boston University, and runs of both impulsive and periodic-type disturbances have been made. The purpose of this modeling study is to determine whether the morphology of the perturbed model ionosphere matches that of the real ionosphere. This would in turn establish that a modeling study can be utilized to enhance our understanding of the ionospheric response to different situations, via further diagnostic modeling studies.

In the next two sections, the modeling of the ionospheric response to impulsive and periodic disturbances, respectively, are described.

2.1 Storm Onset

A number of authors over the years have examined the ionospheric response to geomagnetic storms. Some have summarized the climatology of the response in a global sense (e.g., Davies, 1974; Rishbeth, 1975; Rishbeth et al., 1978; Fuller-Rowell and Rees, 1981, Fesen et al., 1989) discussing the roles played in the storms by impulsive heating and global circulation. Others have studied the reponses in more detail but at limited locations (e.g., Mendillo et al., 1972; Titheridge and Buonsanto, 1988; Wrenn and Rodger, 1989; Fox, 1990) with a view to describing and predicting the likely response to a given storm.

The problem of modeling the ionospheric reponse to geomagnetic activity has been examined more closely in recent years. The Storm group of CEDAR has focussed

attention on two storm periods and a number of modeling groups are active in attempting to model the observed ionospheric response. In addition, Fuller-Rowell et al. (1991) demonstrated that strong heat influx at high latitudes can lead to significant increases in the molecular mass at middle latitudes, leading to the observed negative phase of storms in that region. At lower latitudes, Fesen et al. (1989) modeled the ionospheric response to a changed thermosphere and circulation model (but, importantly, ignoring electric field effects) for the March 22, 1979 storm. The NCAR model indicated that large-scale waves propagate equatorward, and that the derived variations in Nmax and Hmax (that agree fairly well with observations) are mostly due to resulting changes in the meridional neutral wind.

In this study, the goal was to adapt the Phillips Laboratory GTIM to the study of storm onset and to validate the adapted model by comparisons with observed storm response characteristics. The approach adopted varied with the latitude region of interest:

- at middle latitudes, the dominant influence on the ionosphere is the thermospheric composition. The storm-time variations seen in the MSIS-86 (Hedin, 1987) model used in GTIM have been previously studied and were seen to be broadly consistent with observations.

- at low latitudes, changes in composition with Ap are minimal, but there are significant changes according to the ambient vertical drift field that does change in geomegnetically active periods. As this variation has not yet been described in the literature, some work was performed here in order to summarize the existing observations. This is outlined in the next section.

2.1.1 Low Latitude Storms

The first step in determining what changes to vertical drift patterns are related to geomagnetic activity was to refer back to the published **E x B** drift patterns at

Jicamarca of Fejer (1986) and Fejer et al. (1989, 1991). These databases cover some geomagnetically active periods. While there is significant day-to-day variability in these published drift patterns, some average, or at least, most likely, magnetic activity effects could be discerned. Perturbations to the drift patterns that seemed to best summarise the changes in the Jicamarca patterns occurred:

(1) at the pre-reversal (or post-sunset) enhancement (PRE)

(2) towards the daytime peak (0900-1400LT)

(3) towards the nighttime minimum (0000-0500LT).

The PRE change applied was a scaling factor, typically 50%, while the changes to daytime and nighttime values were taken to be linear offsets of typically $20 ms^{-1}$, but reduced somewhat in the solar minimum model runs. Because the PL GTIM applies this drift pattern over the whole low latitude region (i.e., over both hemispheres), the patterns are assumed to apply to a month rather than to a season when extending these changes derived at Jicamarca to other longitude sectors (note that the Asian sector drifts were taken to be the Pacific sector values, derived for the PRISM model of Daniell et al. [1994]).

Because the interest here was in validating the use of the GTIM for storm studies, a grid of modeling runs should ultimately be performed. These involve achieving a model ionosphere according to the climatological vertical drift pattern up to the desired Local Time (the onset time of the storm, as it were), then following the model as the drift pattern changes to that expected for geomagnetically active conditions. The concern here is the modeling of this period following storm onset; no subsequent relaxation back to the climatological vertical drift pattern has been considered.

Some examples of the modeling performed to date are given in Figures 1-4. Each of the figures corresponds to the TEC variations observed at six selected latitudes for

a particular onset Local Time (00, 06, 12 and 18LT, respectively in the figures). The solid line in each plot shows the diurnal variation of TEC under normal conditions (here Equinox, Solar Maximum) while the dotted (and dashed) line shows the values obtained from the model in the first (and second) day following onset. The trends seen in these figures are:

- that overall, the effects at low latitudes predicted by the model are not sensitive functions of the storm onset Local Time

- that typically, morning values of TEC are higher during magnetically active periods

- that typically, afternoon values of TEC are lower during magnetically active periods

- that the phase of the storm in the evening sector depends on the location of the site; inside the equatorial anomaly region, the model phase is positive, while outside, it is negative.

The above factors are consistent with the idea that the time taken for the model to adjust to the disturbed vertical drift pattern is quite short. Further, there is no obvious initial response in the model ionosphere, suggesting that possibly some impulsive change to the model vertical drifts would be required for a more rapid response. Comparisons with data will be undertaken to determine the important features sought in this modeling study.

It should be pointed out that this study cannot be conducted reliably for L shells of 1.03 or so (note that no equatorial results are presented in Figures 1-4). In the presence of vertical drift, the ionization present on a given field line at the start of the modeling may drift to a point below which the model is not reliable (say, 150 km altitude), at which point the simulation is stopped. To fill out the equatorial coverage for the background conditions, it is simply necessary to begin the simulation at different (staggered) local

times and to follow each for as long as possible. However, to begin a modeling study of particular field lines from particular onset times restricts the results to those L values that never drift to lower than 150 km in the perturbed drift field (equivalently, restricts the time that can be modeled following storm onset).

2.1.2 Middle Latitude Storms

For middle latitude runs, the middle latitude component of the GTIM, known as MIDLAT, was run up to a particular Local Time (again, effectively, the onset time of the disturbance). After that point, an Ap history file that defines the storm is included, and it is this that drives the thermospheric models within GTIM. Each of the neutral wind (Hedin et al., 1988) and composition (Hedin, 1987) models uses a series of Ap values, from the current 3-hour value to an average of the previous few days, and these values are calculated at each time from this storm history file.

For the reason that the Ap history file is so specific, it is difficult to prepare a comprehensive grid of model runs. However, a number of case studies have since been conducted, contrasting the results of storm phases from the modified GTIM with measurements of total electron content (TEC) observed in Hamilton, MA. To drive the model for these case studies, initial conditions are first achieved by setting a constant Ap value of 3. Examples of case study comparisons for the deviation in percentage TEC from "quiet-time" values are presented in Figures 5 and 6, concentrating on the departure from ambient conditions expressed as a percentage. In each figure, the storm-time data from Hamilton, MA, is denoted by the solid line, while model results at three different latitudes are included as dotted, dashed and dot-dashed lines. There is often a good level of agreement provided by the modified GTIM. Consistently the most difficult "features" to describe by the model are rapid variations (timescales of two hours or less), and those occurring in the nighttime (specifically, predawn) hours when the theoretical model is

not always able to maintain the ionosphere, and the background description is therefore not as reliable. The storm response in the model is seen to be a fairly rapidly decreasing function of latitude in this latitude range. The overall level of agreement between model and observations will also be modified by other factors that induce day-to-day variability in the ionosphere. For example, in Figure 6, the storm-related effects on the day of onset are fairly well-described by the model, but the following two days of data do not show any significant daytime effects, implying that some other factor is suppressing the anticipated daytime excursions.

An alternative means of testing the predictions of the storm-time ionosphere using the modified GTIM is to compare it with the predictions of the empirical storm-time response model of Fox (1990). This model is probabilistic in nature, being a summary of some 400 storms from Hamilton, MA, observations of TEC. In that sense, it provides some climatological basis for comparison. Comparisons between the empirical and theoretical model predictions were then made over a grid of conditions (season, solar activity level, onset local time and peak Ap value). The agreement between these two approaches was seen to be more qualitative than quantitative. The empirical model consistently predicted larger and more rapid responses than the theoretical model, but generally the estimation of positive and negative storm effects in the theoretical model was consistent with the empirical model.

While there may be conceptual problems with simply perturbing mean thermospheric models to drive the storm response of an ionospheric model, the good level of qualitative agreement between the modeled and observed response does strongly suggest that thermospheric influences are dominant in the middle latitude disturbed ionosphere, and that MSIS provides a plausible foundation for this work.

2.2 Ionospheric Waves

Recent analyses of observations taken at low latitudes have revealed significant periodic variations, potnetially a significant factor in "day-to-day variability". Forbes and Leveroni (1992) described a 16-day apparent periodicity in foF2 data taken from Huancayo, Peru. Ongoing work (Parish, 1994) concerns the search for periods of the order of two days in data from a network of ionosondes at several longitudes.

To study ionospheric waves, an additional version of the GTIM was developed. In this case, the model would be allowed to converge to background conditions in the manner of the storm-onset version, described above. Then, at a specified "onset" time, a wave-like perturbation on the background vertical drift field was applied, with the simulation results being monitored for at least two wave periods. The perturbation itself is ither expressed as a percentage change of the background pattern, or in absolute terms, being a wave of a certain number of ms^{-1} The pertubation of the wave would be 0 at the onset time (i.e., the variation is sin-like, rather than cos-like), and can be set to be a positive or negative change from that point. The GTIM at low latitudes is run at specified longitude locations, rather than being a consistent global specification. For that reason, runs made at other longitudes should be coordinated according to the assumptions made about the global onset of such waves. Considerations, such as whether a wave is begun at the same Universal Time globally, what the wave number of the perturbation wave would be (and therefore whether variations are in phase or not at different longitudes) will determine what input conditions are used for the separate longitude runs.

For the reason that it was considered better to develop and optimize the code for the shorter period modeling runs purely from time considerations, more work performed thus far has concerned the study of two-day waves.

A specific case study undertaken was for the end of August, 1979, primarily in

the East Asian longitude sector, as that was where the most station data was available, and thus a better estimate of the background conditions could be m Stations available, with dip latitudes in parentheses, were Akita (30°), Mani), Okinawa (16°), Yamagawa (20°), Townsville (−28°), and Canberra (−44°). While wave-affected conditions at Manila cannot be studied, owing to the issue discussed at the end of section 2.1.1, the determination of background conditions still may be enhanced with the additional data.

It is first necessary to describe the ambient conditions with the model. There are significant day-to-day variations in the diurnal variations of vertical drifts (Fejer et al., 1991), so it is unreasonable to expect the climatological average patterns to apply to any particular date, and thus a series of model runs were made. It was apparent that the significant level of post-sunset enhancement that would be expected for equinox, solar maximum conditions was not present at all in the real ionosphere (stations near the anomaly crest showed no evening peak in foF2). Selected diurnal variations are shown in Figure 7. Additionally, the shapes of the diurnal curves of foF2 in the data showed a more rapid rise after sunrise and a more gradual decrease from the maximum than was obtained in the model and the "background" was adjusted accordingly. The derived diurnal variations at selected latitudes are shown in Figure 8 and reasonable agreement is obtained overall with the average variations shown in Figure 7.

An example of the output of one such model run is seen in Figure 9. This displays the "background" diurnal curves of foF2 together with the wave-time variations over two periods at four selected (dip) latitudes. The wave in this case was an absolute amplitude (3 m/s, around 10% of the total amplitude), onset at 2100LT variation. The following effects are noted:

- That there is no discernible effect at a latitude of 30 degrees, consistent with the

observations.

- That effects are largest (and importantly, in phase) at 16 and 20 degrees, also consistent with the observations.

Additional runs are still in progress.

Some exploratory runs have also been performed for a wave of 16-day period, and one form of output is shown in Figure 10. This displays the day-by-day variation of the 16LT value of foF2 at selected latitudes (together with the background value, seen as a straight line), and shows that the variation therein is also sinusoidal. This is important as it indicates that wave-like changes in vertical drift patterns of longer periods will yield wave-like changes in observable quantities. The relatively large variations in this figure, compared to Figure 9, say, arises from the large amplitude used for the wave (50%, relative amplitude).

3. EXTENSIONS TO THE PRISM MODEL

A recent collaborative modeling effort undertaken in the Boston area produced both the Parameterized Real-time Ionospheric Specification Model (PRISM) and the Parameterized Ionospheric Model (PIM) (Daniell et al., 1994). These are parameterized versions of a grid of theoretical model runs (PIM) that could adjust the global ionosphere in the presence of a variety of available real-time data (PRISM). While validation runs conducted thus far have been encouraging, a primary limitation of the model is that being largely based on the GTIM, it is limited to O^+ ions in the topside. A necessary addition to this effort was thus to include a plasmaspheric component in the parameterization. The model originally described by Bailey and Sellek (1990) and recently updated in Bailey et al. (1993) is well-suited to this purpose, in that it affords a model plasmaspheric specification with many of the same inputs that are used in the GTIM.

3.1 Description of the Bailey Model

The Bailey model determines solutions for a variety of ions (O^+, H^+, He^+, N_2^+, O_2^+ and NO^+) that satisfy time-dependent equations of continuity, momentum and energy balance. The model extends from a base altitude of 150 km to the plasmapause. Like the GTIM, this model determines solutions to the diffusion equation along magnetic field lines. The same thermospheric description (Hedin, 1987; Hedin et al., 1988) and magnetic field model is used as a basis. The plasmaspheric component of this model requires a number of simulation days (ten or more) to fill the plasmasphere. It is envisaged that the intermediate stages of runs for this model would provide different levels of refilling of the plasmasphere that could be used in the next level of PIM/PRISM parameterization, in terms of the number of days since the previous geomagnetic storm (that is assumed to empty the plasmasphere).

Additional routines have been prepared to provide output from the Bailey model in the same format as provided by GTIM, in order to expedite comparisons between the models. Further controlling software was written to enable model runs to be generated over a wide range of field lines and non-uniform spacings of L shells. This latter allows greater flexibility to optimize the location of the electron density products that are to be parameterized.

3.2 Model Validation and Comparisons

Prior to there being detailed intercomparisons between the GTIM and Bailey model output, a number of changes to the latter model were required for internal consistency with the model parameters established for PRISM (Daniell et al., 1994). In point form, these changes included:

- replacing the reaction rates and cross-sections to those values used for PRISM.

- generalization of the usage of **E x B** drift patterns to allow usage of the same files prepared for the PRISM grid. The best altitude variation of these drift patterns out to the greater plasmaspheric altitudes has not yet been determined.

- replacing the section that determines electron and ion temperatures from the heat balance equations with the simple model (Brace and Theis, 1981) preferred in PRISM. This speeds up the model run-time considerably.

- ensuring that all the calls to the thermospheric specification routines are the same in two models.

- providing solar flux input that can be used by the Bailey model but that is derived from the Hinteregger et al. (1981) flux model preferred in PRISM. Similarly, a version of the low latitude GTIM was prepared that can use the same cross sections and solar flux model (Tobiska, 1993) that are preferred in the Bailey code.

- including additional ion "switches" for the light ions, H^+ and He^+, to make it possible to seek purely O^+ solutions in both models, while also switching off molecular ions in the Bailey model.

- altering the parameter that determines where along the field lines the solutions to ion densities are sought.

It has been verified to date that the neutral densities, neutral and ion temperatures, and O^+ loss rates are indeed the same in both models. The rates of O^+ production in the two models still differ. This stems from the following factors:

- that nighttime production is treated differently in each model. In GTIM, the production rate is artificially scaled up by large factors to maintain the nighttime ionosphere. In the Bailey model, the production rate is scaled down by a large factor from the noontime value.

- that GTIM includes secondary photoionization, and this can be a significant contributor.

Some examples of detailed comparisons between the models generated for the US Sector, Equinox and Solar Moderate conditions are given in Figures 11 and 12. These runs are based on the solar flux model and photoionization cross sections preferred in the Bailey model. The plots on the left side of the page define the L shell being portrayed and the N rows of plots represent N Local Times. Daytime hours are shown here, owing to the still-present differences in the nighttime production formalisms. The right hand plots are latitude-compressed profiles (i.e., O^+ densities along the field line) where the southern hemispheric portion of the fieldline is made negative for clarity in the plot. The different line styles in the Figure 11 corresponds to: Solid line = Bailey model output; Dotted line = GTIM output, direct photoionization only; Dashed line = GTIM output, direct and secondary photoionization; Dot-Dashed line = GTIM output, direct photoionization and photodissociation. It can be seen that the secondary and photodissociative terms are very similar in magnitude. The different line styles in the Figure 12 corresponds to: Solid line = Bailey model output; Dotted line = GTIM output, direct photoionization only; Dashed line = GTIM output, direct photoionization and photodissociation; Dot-Dashed line = GTIM output, direct and secondary photoionization and photodissociation. The overall agreement between the sum of terms in GTIM and the Bailey code is reasonable, but there are differences that still need to be isolated and that are seen to vary with Local Time. The form of the nighttime production in the Bailey model has not yet been changed.

4. EQUATORIAL IONOSPHERE STUDY

A number of low latitude ionospheric studies have been published in recent years that address the issue of the origins of spread-F conditions (equally, scintillations) and how the observed occurrence rates of spread-F come about. Tsunoda (1985) comments on the maximum scintillation occurrence coinciding with the times when the E-layer conductivity is changing most rapidly. Maruyama and Matuura (1984) interpret the longitudinal variations of spread F conditions in terms of variations in the meridional neutral wind. Mendillo et al. (1992b) contrast these works and point out the different emphasis in terms of conditions that either instigate or suppress spread-F. They further examine the growth rates of spread-F and the "capricious" role that may be played by surges in meridional winds. In each case, the level of hemispheric symmetry in electron density is of primary concern.

It was thus considered useful to undertake a modeling study of symmetries and asymmetries in the low latitude GTIM ionosphere, with a view to

1. establishing that the asymmetries in the model are consistent with the observed spread-F morphology, summarized in the next section, and then

2. using the model to investigate the dependencies of the asymmetries on various external factors (changes in neutral winds, magnetic activity etc.).

4.1 Spread-F Morphology

Aarons (1993) presents a convenient summary of the current knowledge of the longitudinal morphology of spread-F, and a discussion of how the ideas of Tsunoda (1985) and Maruyama and Matuura (1984) may explain this morphology. The principal features of the longitudinal morphology are:

- that equinox months are associated with relatively high spread-F occurrence at all

longitudes

- that the July-August period has relatively high occurrence in the Pacific sector, and relatively low occurrence in the Atlantic sector

- that the November-December period has relatively low occurrence in the Pacific sector, and relatively high occurrence in the Atlantic sector.

It is the interplay between the seasonally varying quantities and the role played by magnetic declination at different longitudes that should provide the key.

4.2 Modeling Asymmetries

In order to gauge how successful the GTIM can be in describing spread-F morphology, as outlined in Aarons (1993), model runs at several longitude sectors were generated. As the only available vertical drift patterns (prior to the imminent publication by Bela Fejer on a longitude dependent drift model) were the US sector climatological averages, and some equivalent drift patterns developed by Anderson (1992, private communication) for use in the Pacific sector, the nearest applicable sector values were those used in general for this study. The sectors chosen here were: Indian at 80° E, Asian at 120° E, Peruvian at 285° E, and Natal at 305° E. In order to establish the climatology at each sector, runs were made for each two months of the year for solar maximum (1981), in order to magnify the anticipated effects.

Summary contour plots of electron density were generated at 2100LT (selected as a representative post-sunset time) for each sector, and these are shown in Figures 13-16. These are a convenient means of demonstrating the level of symmetry in the local ionosphere, and in turn permit comparisons with the observed spread-F morphology. Overall, the level of consistency with model ionosphere asymmetries and observed spread-F is quite good. Figure 17, taken from Aarons (1993) is used as a convenient summary of

the observational trends.

For example, taking Manila as an Asian sector station, peaks in spread-F are seen in the equinoctial months in Figure 17, and in Figure 13, the most symmetric distributions of Ne are also seen in those months (3 and 9). Further, the greatest asymmetry in Figure 13 is in months 1 and 11, consistent with the minimum in spread-F in Figure 17. In Figure 14, the results for the Indian sector model runs in comparison with data from Kodaikanal show the same results and the same level of agreement (consistent with the similar magnetic declination at the two locations). The results of the Peruvian sector (Figure 15) runs are similarly consistent with spread-F morphology from Huancayo, but unlike the earlier two sectors, show a minimum in spread-F (and maximum asymmetry) in the June solstice. Natal, at the location of large magnetic declination, does not show (Figure 16) the same level of modeling success. In that case, the Natal sector results were regenerated using a hardwired higher declination of -20 degrees, rather than relying on the declination provided by the simple magnetic field model within GTIM. These are shown in Figure 18. Here the agreement with spread-F morphology is improved. The months with the highest symmetry in Ne are now 1 and 11, coinciding with the peak in spread-F, with greater asymmetries in the other seasons.

This indicates that the GTIM is a plausible place to study spread-F/irregularities. These climatological studies are based on the thermospheric wind fields of Hedin et al. (1988) and measured wind values should be used whenever possible for case studies because the level of symmetry in the low-latitude ionosphere is sensitive to the chosen neutral wind field.

4.3 The Effects of Magnetic Activity

As outlined in Section 2.1.1 of this report, the most likely changes to vertical drift patterns in the presence of geomagnetic activity can be tentatively identified. These

same active vertical drift patterns can be used to estimate the effects on hemispheric asymmetries (and thereby on spread F occurrence rates).

Results obtained for active periods in the Asian sector are shown in Figure 19. Overall, the changes to the size and location of the anomaly crests at all seasons do not shift the seasonal pattern displayed for quiet-time densities (seen in Figure 13). The seasonal pattern of asymmetry (and therefore inferred for spread-F) is not apparently affected by magnetic activity (i.e., and should be reproducible). Rather, it is the degree of hemispheric asymmetry in the model ionosphere that is changed. How this is interpreted in terms of magnetically active periods occurrence rates for spread-F would then depend on how one chooses to define the degree of asymmetry (e.g., a ratio of densities at constant heights and latitudes, a difference in heights at constant density and latitude, density ratio of the anomaly crests, height difference in the anomaly crests). The best parameter for this purpose has not yet been determined.

5. SUBSTORM MODELING STUDY

In this section, the GTIM has been used to simulate total electron content (TEC) disturbance events observed at middle and lower latitude sites near 75°W and 7°E longitudes during substorms. Within this longitudinal range, the daytime TEC disturbances show a pattern in which a positive response can be followed by a negative response or depletion, or diurnal double maxima (DDM) patterns if substorm activities are repeated. The required dayside electric fields in both longitudes show eastward and westward perturbations during substorm expansion and subsidence phases, respectively. This is suggestive of magnetospheric electric field penetration and subsequent overshielding effects as the responsible mechanism. The morphological features of the required electric field perturbations near dawn and dusk are compared with those at other times, to examine the local time characteristics of magnetospheric influence.

Large scale traveling atmospheric disturbances (TADs), as an alternative candidate for the disturbance source, are also investigated and compared with known thermospheric characteristics.

5.1 Introduction

Recent studies have shown that ionospheric disturbances, including variations in electron density, its height distribution and total electron content, at middle and lower latitudes during substorms have characteristic features that differ from effects associated with major magnetic storms (e.g., Reddy et al., 1990; Prölss et al., 1991; Pi et al., 1993). These differences can be attributed to the degree of temporal continuation of coupling processes between the magnetosphere, ionosphere, and thermosphere. While major magnetic storms have long-lasting effects on global thermospheric circulation, composition, and electrodynamical changes (e.g., Rishbeth, 1975; Mendillo et al., 1992a), substorms can be the origins of shorter period ($\sim$ hours) electric field perturbations and thermospheric dynamics. These include penetration and overshielding of magnetospheric fields (e.g., Vasyliunas, 1972; Kelley et al., 1979; Spiro et al., 1988; Fejer et al., 1990], as well as large scale traveling atmospheric disturbances (TADs) (e.g., Prölss, 1993). The degree to which these short duration disturbance processes also affect the ionosphere on a global scale is uncertain. Here, we address the issue via modeling studies of F region variations observed during individual substorms.

5.2 The Observed Events at Two Longitudes

TEC observations had been made continuously since the 1970's at many sites near 75°W by the U.S. Air Force Phillips Laboratory, and near 7°E by the IROE ionospheric research group in Florence, Italy. The Florence site has the same geographic latitude (39°N) as Hamilton, but a dip latitude (35°N) closer to Kennedy Space Center (KSC)

(38°N). These sites were selected for study because the geomagnetic control of the ionosphere at Florence may be similar to that at KSC, while its solar production and thermospheric environment have a higher latitude signature more like the Hamilton location.

It is found through examining TEC data sets that the DDM pattern is one of the typical ionospheric disturbances that is present in both the American and European longitude sectors. Examples of this disturbance pattern, observed at these middle and lower latitude sites during periods of substorm activity, are plotted in Figures 20 and 21. The AU/AL and Dst indices give auroral electroject and ring current behavior, respectively. It is clear that no major magnetic storms occurred during the period. In Figure 20, the Florence data show the typical DDM pattern described in detail in the earlier study of Pi et al., (1993). This DDM pattern did not develop similarly at the American longitude sites (about 5 hours difference in local time) because the substorms did not correspond to postsunrise/prenoon and postnoon/presunset local times at 75°W. The counterexample is shown in Figure 21. On January 31, 1981, corresponding to two substorms during 9-12UT and 19-23UT, TEC pre and postnoon DDM appeared at the American longitude sites, though it is less obvious at Hamilton. At Florence, a TEC noontime increase occurred following 10UT substorm but not following the substorm at 20UT, after local sunset.

5.3 Modeling TEC Disturbances

Qualitatively, the TEC disturbances shown in the last section can be caused by dynamical sources due to substorms that affect the balance between local production and loss mechanisms. One of the characteristics of such disturbances is that while dynamical effects move plasma into different height regions, implying only a TEC-preserving $N_e(h)$ redistribution, the TEC actually responds with a time delay associated with chemical

reaction time constants in the various height regions populated by the new distribution. This delay of the TEC responses can be seen particularly well in the case of January 31, 1981, at all sites, following the 10UT substorm.

The ambient state of the ionosphere must also be taken into account in longitudinal comparisons of TEC disturbances. This is due to the fact that longitudinal differences in the background ionosphere, which are mainly determined by solar photoionization and neutral winds, may make TEC disturbances appear significantly different for similar driving sources. The following ionospheric modeling studies deal with both background and disturbed conditions. For disturbed conditions, electric fields and impulsive winds are considered separately in order to gauge quantitatively the sensitivity of the F region to these individual mechanisms.

It is first necessary to set up the GTIM to model the background conditions, prior to studying stubstorm effects. The model is applied to investigate how the ionosphere at Ramey, Kennedy Space Center, and Florence respond to the disturbance sources. With the model so established, simulations of TEC disturbances can then be conducted by introducing electric field or neutral wind disturbances.

For the case of July 30, 1982, the background TEC control curve is represented by the 31 day average values centered at the event day. As the model initially yielded different TEC mean values than were observed at all three sites, additional meridional winds were introduced. The major wind adjustments are extra poleward components that are added during day time hours at all three sites, while the equatorward wind at the American longitude is enhanced for post midnight hours. It needs to be pointed out that although these wind adjustments are required for the model to fit diurnal observations, they are not crucial to the shorter local time patterns of disturbance. Alternative adjustments to the model (lowering solar fluxes or increasing MSIS molecular abundances)

are less attractive solutions because dynamics, rather than production/loss processes, are the major uncertainty sources in matching observed morphologies.

With the control curves reproduced to a satisfactory level, the model was run under the event day conditions to examine possible electric field disturbances associated with substorms. Figure 22 gives the modeling results for the required zonal electric field perturbations at the three observing sites. Figure 22 also includes the auroral electrojet *AU/AL* and magnetic *Dst* indices, as well as the TEC mean values from both observation and modeling, to show the context of substorm activity effects on this day. In addition, the major substorm activity on July 30, 1982, is divided into three periods (labeled (1)-(3) in the figure) to separate a subsided substorm interval (period (2)) from two major substorm events (periods (1) and (3)). In each period, the zonal electric field disturbances that are required to produce the TEC DDM disturbances observed at Florence, show the typical dayside penetration-overshielding-penetration pattern discussed in Pi et al., (1993).

In the US sector, as shown in Figure 22, the required electric field perturbations have larger magnitudes during the noontime period, as compared to those at dawn and dusk. These seem to be consistent with the picture of a simple dawn-dusk magnetospheric electric field in which the field magnitudes of the zonal components are smaller at dawn and dusk. However, this simplified scenario is not sufficient to explain the requirements at the Florence site where a considerable eastward electric field perturbation is required around dusk corresponding to substorm period (3).

The overall requirements of electric field magnitudes given in Figure 22 show a decreasing trend from higher to lower latitudes, consistent with the penetration-overshielding assumption. However, the durations of the required electric field perturbations at certain times seem to be longer ($>$ 4 hours) than those shown in Pi et al., (1993). A discrepancy between the two longitudes is that the duration of required

westward (overshielded) electric field perturbation is much shorter at KSC (and essentially not present at Ramey) during the post sunrise hours, while it is prominent at mid-day in Europe during period (2). Overshielding effects are seen at all three sites following substorm period (3).

The case of July 30, 1982, can also be modeled with enhancements of thermospheric winds, or impulsive large-scale TADs, added to the background winds. The equatorward TADs required for uplifting the F layer to regions of reduced loss can be attributed to the substorm periods (1) and (3). Yet the temporal/latitudinal coherence varies with longitude. Poleward TADs are required to produce daytime TEC depletions at Florence and KSC, but only a small amplitude TAD is required at Ramey. These poleward TADs, presumably propagating across the equator from the southern hemisphere, show no evidence of damping. Rather, the amplitude of the derived TAD at 14UT shows an increase from Ramey to KSC.

5.4. Discussion and Conclusions

The ionospheric positive response to substorms has long been suggested to be due to TADs (historically as TIDs - travelling ionospheric disturbances referring to the ionospheric observations) in middle latitudes. The observed evidence is the time delay (a few hours) of the ionospheric peak height behavior at middle latitudes relative to substorm activity shown at high latitudes, attributed to TAD propagation (e.g., Prölss, 1993). This characteristic was required neither by Pi et al., (1993) for the selected ionospheric disturbance cases, nor in the present study. This raises the possibility of other dynamical sources which can rapidly affect the global ionosphere, such as elctrodynamic effects. In addition, the TAD mechanism for producing observed TEC disturbances also needs to address the reversal issue of TAD's appearing from the opposite hemisphere as substorms subside, as well as their long duration and very rapid propagation speeds. Recent evidence

of substorm effects in the low-middle latitude ionosphere obtained from incoherent scatter radar measurements (Buonsanto and Foster, 1993), shows that a more complete picture of substorm disturbance mechanisms may be drawn by understanding the interplay between magnetospheric electric fields and neutral winds.

In conclusion, we have identified a consistent daytime ionospheric disturbance pattern at middle and lower latitudes during substorms: an ionospheric TEC positive response corresponding to substorm expansion periods, followed by a depletion or negative response as the substorm subsides. Observations show that this basic pattern can occur at longitudes that differ by at least five hours. Ionospheric modeling studies reveal that the requirements for the electric field disturbances are consistent with a penetration and overshielding assumption within the longitudes investigated here. The required magnitudes (0.5-1.0 mV/m) of electric field perturbations at latitudes investigated here are also consistent with fields measured by incoherent scatter radars and modeling results of magnetospheric electric field penetrations. The latitudinal gradient of the required electric field magnitudes also shows a consistency with basic penetration and overshielding assumptions in which the magnitudes decrease toward lower latitudes.

This work in this section is being submitted to Journal of Geophysical Research, as Longitudinal Effects of the Ionospheric Responses to Substorms at Middle and Lower Latitudes: A Case Study, by X. Pi, M. Mendillo, P. Spalla and D. Anderson.

6. NEUTRAL DENSITY WAVES

6.1 Small-Scale Waves

SETA density measurements (normalized to a nominal altitude of 200 km) were analyzed to delineate characteristics of relatively small-scale waves (horizontal structures of order 100 to 2,000 km) in the data. The spectral analyses were applied to all available

orbits (approximately 15 to 18 per day) during 6 days in 1983 and 10 days in 1982, covering a range of geomagnetic conditions.

The 1983 density measurements were taken once every 4.09 seconds corresponding to a rate of 0.244 Hz. The effective Nyquist rate is therefore 0.122 Hz which translates to a minimum identifiable horizontal wavelength of 8.2 km. In the case of the 1982 data, density measurements were taken once every 20.45 seconds corresponding to a rate of 0.049 Hz. The effective Nyquist rate is therefore 0.024 Hz. This translates to a minimum identifiable horizontal wavelength of 40.9 km for the 1982 data.

Much of the past year of activities have been devoted to pre-processing the satellite data, and developing an applying various spectral methods to the data set. The following describes the methods of analysis which were developed, along with sample results from the analysis.

6.1.1 Spectral Analysis

Standard periodogram spectral analyses were applied to each orbit of uninterrupted data. The orbits were categorized into three levels of magnetic activity in order to determine the dependence of periodicities on the magnetic activity. The categories are (a) quiet: $\mathrm{Kp} \leq 2$; (b) average: $2 < \mathrm{Kp} \leq 4$; (c) active: $\mathrm{Kp} > 4$. In this section we describe the results of periodogram spectral analysis performed on the density data.

The periodogram spectral analysis is based on estimating the distribution in frequency of the power $P_x(w)$ or the *power spectral density* (PSD) of a random signal $x[n]$ (density measurements in this analysis). This quantity can be shown to be related to the squared magnitude of the Fourier transform of the signal $x[n]$ by an extension of the Wiener-Khinchin theorem (Kay, 1981) as follows:

$$P_x(w) = \lim_{M \to \infty} E\left[\frac{1}{2M+1}\left|\sum_{n=-M}^{M} x[n]e^{-jwn}\right|^2\right] \quad (1)$$

where $E[.]$ denotes the expectation operator. Neglecting the expectation operator, the PSD of the signal $x[n]$ of length N may be estimated as:

$$\hat{P}_x(w) = \frac{1}{N}\left|\sum_{n=0}^{N-1} x[n]e^{-jwn}\right|^2 \quad (2)$$

which is the squared magnitude of the Fourier transform of $x[n]$ and can be evaluated using the FFT algorithm.

PSD's were generated for each uninterrupted orbit in the data base using 4096-point FFT's. Since each orbit of the satelite takes approximately 90 minutes, 1296 data points were analysed for each orbit in the case of the 1983 measurements.

6.1.2 Periodogram Averaging

The power spectra can be estimated more "reliably" by attempting to approximate the expectation operator described in the previous section. The technique is known as periodogram averaging and it is described in the following.

Suppose that $\hat{x}_1[n], \hat{x}_2[n], ..., \hat{x}_K[n]$ are K uncorrelated instances (data records) of the same random signal $x[n]$. The *averaged periodogram* (Kay, 1988) is then defined as:

$$\hat{P}_{avg}(w) = \frac{1}{K}\sum_{m=1}^{K} \hat{P}_m(w) \quad (3)$$

where $\hat{P}_m$ is the m^{th} periodogram given by:

$$\hat{P}_m(w) = \frac{1}{N}\left|\sum_{n=0}^{N-1} \hat{x}_m[n]e^{-jwn}\right|^2 \quad (4)$$

which is the squared magnitude of the Fourier transform of the m^{th} data record $\hat{x}_m[n]$. The variance of the averaged periodogram can be shown to be decreased by a factor of

K while its expected value remains the same as the true PSD. In this sense the averaged periodogram is a more reliable estimate of the power spectrum.

Our averaged periodogram analyses are twofold. First, the average of the spectra for all of the uninterrupted orbits in each day is calculated. Second, the orbits are categorized into three levels of magnetic activity as described in the previous section, and for each level of magnetic activity an averaged periodogram is calculated.

The averaged periodogram corresponding to quiet and active orbits during the six days in 1983 are illustrated in Figure 23. This illustrates the enhancement in wave activity, especially at wavelengths longer than 1,000 km, which is generated in conjunction with magnetic disturbances.

Similarly, a comparison of day vs. night periodograms for all orbits during 1983 are illustrated in Figure 24. This plot illustrates the enhancement in wave activity which occurs at scales shorter than 400 km during the night, whereas the spectral densities at wavelengths longer than 500 km are virtually the same. We do not have a definitive explanation for this result as yet.

6.1.3 Wavelength Contribution to Signal Energy

In order to gain quantitative insight into the contribution of various wavelength ranges to the total signal energy, an equation known as Parseval's relation may be utilized, which relates a signal's total energy to its total spectral energy (Oppenheim and Schafer, 1989) by:

$$\sum_{n=-\infty}^{\infty} |x[n]|^2 = \frac{1}{2\pi} \int_{2\pi} |X(w)|^2 dw \qquad (5)$$

where $x[n]$ is the discrete-time signal corresponding to the data values, and $X(w)$ is the spectrum of the signal. The quantity on the left-hand side of the equation is the

total energy in the time-domain signal $x[n]$, and $|X(w)|^2$ is referred to as the *energy-density spectrum*. The quantity of interest here, which we refer to as the "percentage contribution", is the ratio of the energy in an arbitrary wavelength range to the total signal energy. According to Parseval's relation this quantity is proportional to the ratio of the energy in the arbitrary wavelength range to the total spectral energy. Since the wavelengths of interest here are all in the range of 0 to 2500 km, the "total" energy may be replaced by the energy in the range of 0 to 2500 km. The percentage contribution may therefore be defined as the ratio of the energy in an arbitrary wavelength range to the total energy of the signal with wavelengths between 0 and 2500 km. The averaged periodogram results described in the previous section are used to compute the percentage contribution for the density data during 1983 as a continuous measure of the ratio for all wavelengths in the range of 0 to 2500 km. The percentage contributions of the wavelengths are therefore both equal to 0% at 0 km and 100% at 2500 km, and increase continuously with increasing wavelength. Results of this type of analyses were provided in the first two quarterly status reports of the current annual reporting period.

6.2 Large-Scale Waves

Two pre-processing methods are being applied to the same 1982 and 1983 SETA data in order to investigate larger-scale (planetary wave) oscillations in total mass density. The impetus for this investigation originates in 2-, 5-, 10-, and 16-day oscillations being discovered in various other wind and ionospheric data sets. The first pre-processing method, SETA Processing for Least-Squares Analysis (SPLSA), is described below. The second, SETA Processing for Asynoptic Sampling Analysis (SPASA), will be reported on in the future. Each of these pre-processing steps leads to a data set which will be analyzed in different ways in an attempt to elucidate and characterize planetary wave signatures in thermospheric density.

In the SPLSA, The different orbits read off the PL VAX MSS were identified and the data were binned into 20 degree latitude ranges (i.e. 0 - 20, 20 - 40, 40 - 60, and 60 - 80 degree latitude ranges, north and south of the equator) and the day and night sections of each orbit were separated. The values of the density normalized to 200 km were averaged for each of these 20 degree latitude ranges, for a given day or night section of the orbit. Values of the density from altitudes above 240 km were taken to be innaccurate and ignored in the averaging process. The averages for each latitude range were formed into time series over 7 months in 1982 and 9 months in 1983-4, (with separate files according to latitude range, northern or southern hemisphere and daytime or nighttime results). Processed results were checked for correctness against the original datasets.

The output files contain the following fields:

Field	Type	Comments
date	int	date and universal time as YYDDD
date	int	decimal fraction of a day x 1.0e4
UT	real	Universal Time (hours)
LT	real	Local time (hours)
long	real	Longitude (0 - 360 degrees)
den	real	Averaged normalised density for given latitude range

A sample plot illustrating the data averaged in this way is depicted in Figure 25. This is a plot of orbit-by-orbit density values which have been averaged between 0 and 20 degreees latitude, in this case daytime data during July 1983. The large excursion on July 4 is connected with a geomagnetic disturbance event. However, it is clear that there exists some repeatable oscillation with an *apparent* periodicity of of 8 - 12 hours which persists throughout the data. Since these data correspond to a single local time,

these oscillations are not connected with the normal migrating tidal oscillations we are familiar with. One possibility is that what we are seeing are not time variations at all, but longitude variations (the earth rotates beneath the satellite once per day). Therefore, these oscillations could be connected with non-migrating tides, or planetary waves with zonal wavenumbers in the range of 2-4. One class of such planetary waves may be Lamb modes, that is resonant oscillations of the atmosphere. We are pursuing these interpretations while continuing to delineate the characteristics of these oscillations through various spectral methods.

The main gaps in the different time series were also located and tabulated. As noted above, the data series described above have both time and longitude as independent variables. This requires special algorithms for processing and interpretation with special attention to the problems of aliasing. The various aliasing problems are presently under study, and analyses of these data will be presented in forthcoming reports.

7. REFERENCES

Aarons, J., The longitudinal morphology of equatorial F-layer irregularities relevant to their occurrence, . *Space. Sci. Rev.*, **63**, 209, 1993.

Anderson, D. N., A theoretical study of the ionospheric F region equatorial anomaly, I, Theory, *Planet. Space Sci., 21*, 409, 1973a.

Anderson, D. N., A theoretical study of the ionospheric F region equatorial anomaly, II, Results in the American and Asian sectors, *Planet. Space Sci.*, **21**, 421, 1973b.

Anderson, D. N., M. Mendillo and B. A. Herniter, A semi-empirical low-latitude ionospheric model, *Radio Science*, **22**, 292, 1987.

Anderson, D. N., J. A. Klobuchar, P. H. Doherty and R. G. Rastogi, A comparison of theoretical modeling of the low latitude ionosphere against TEC data from the Indian longitudes during solar minimum, *Proceedings of International Beacon Satellite Syposium*, Ed. M.-C. Lee, MIT, Cambridge, MA, July 1992.

Bailey, G. J. and R. Sellek, A mathematical model of the Earth's plasmasphere and its application in a study of He^+ at L=3, *Ann. Geophys*, **8**, 171, 1990

Bailey, G. J., R. Sellek and Y. Rippeth, A modelling study of the equatorial topside ionosphere, *Ann. Geophys*, **11**, 263, 1993

Brace, L. H. and R. F. Theis, Global empirical models of ionospheric electron temperature in the upper F-region and plasmasphere based on in situ measurements from the Atmospheric Explorer-C, ISIS 1 and ISIS 2 satellites, *J. Atmos. Terr. Phys.*, **43**, 1317, 1981.

Buonsanto, M. J., and J. C. Foster, Effects of magnetospheric electric fields and neutral winds on the low-middle latitude ionosphere during the March 20-21, 1990, storm, *J. Geophys. Res.*, **98**, 19133, 1993.

Daniell, R. E., W. R. Whartenby, L. D. Brown, D. N. Anderson, M. W. Fox, D.

T. Decker, P. H. Doherty, J. J. Sojka and R. W. Schunk, "The Parametrized Real-time Ionospheric Specification Model, PRISM", Submitted to Radio Science, 1994. Anderson, D. N., A theoretical study of the ionospheric F region equatorial anomaly, I, Theory, *Planet. Space Sci.*, **21**, 409, 1973a.

Davies, K., Studies of ionospheric storms using a simple model, *J. Geophys. Res.*, **79**, 605, 1974.

Fejer, B. G., Equatorial ionospheric electric fields associated with magnetospheric disturbances, **Solar Wind-Magnetospheric Coupling**, ed. Kamide and Slavin, p. 519, 1986.

Fejer, B. G., E. R. de Paula, I. S. Batista, E. Bonelli and R. F. Woodman, Average vertical and zonal F region drifts over Jicamarca, *J. Geophys. Res.*, **94**, 12049, 1989.

Fejer, B, G., R. W. Spiro, R. A. Wolf, and J. C. Foster, Latitudinal variation of perturbation electric fields during magnetically disturbed periods: 1986 SUNDIAL observations and model results, *Ann. Geophysicae*, **8**, 441, 1990.

Fejer, B. G., E. R. de Paula, S. A. Gonzalez, and R. F. Woodman, Average vertical and zonal F region plasma drifts over Jicamarca, *J. Geophys. Res.*, **96**, 13901, 1991.

Fesen, C. G., G. Crowley and R. G. Roble, Ionospheric effects at low latitudes during the March 22 1979 geomagnetic storm, *J. Geophys. Res.*, **94**, 5405, 1989.

Forbes, J. M. and S. Leveroni, Quasi 16-day oscillation in the ionosphere, *Geophys. Res. Lett.*, **19**, 981, 1992.

Fox, M. W., The day-to-day variability of total content, peak density and slab thickness and the ionospheric response to geomagnetic storms, *Air Force Geophys. Lab. Tech. Report GL-TR-90-0313*, Hanscom AFB, Bedford, MA, November 1990, ADA 233294.

Fox, M. W., D. N. Anderson and R. E. Daniell, Determining relationships between

nighttime ionospheric parameters and DMSP-based ultraviolet airglow radiance observations, Submitted to Radio Science, 1994.

Fuller-Rowell, T. J., and D. Rees, A three-dimensional, time-dependent simulation of the global dynamical response of the thermosphere to a geomagnetic substorm, *J. Atmos. Terr. Phys.*, **43**, 701, 1981.

Fuller-Rowell, T. J., D. Rees, H. Rishbeth, A. G. Burns, T. L. Killeen and R. G. Roble, Modeling of composition changes during F-region storms: a reassesment, *J. Atmos. Terr. Phys.*, **53**, 541, 1991.

Hedin, A. E., MSIS-86 thermospheric model, *J. Geophys. Res.*, **92**, 4649, 1987.

Hedin, A. E., N. W. Spencer and T. L. Killeen, Empirical global model of upper thermosphere winds based on atmosphere and Dynamics Explorer satellite data, *J. Geophys. Res.*, **93**, 9959, 1988.

Hinteregger, H. E., K. Fukui and B. R. Gilson, Observational, reference and model data on solar EUV, from measurements on AE-E, *Geophys. Rev. Lett.*, **8**, 1147, 1981.

Kay, S. M., Spectral Estimation, in *Advanced Topics in Signal Processing*, chapter 2, ed. Lim J.S., and Oppenheim A.V., Prentice Hall, Englewood Cliffs, New Jersey, 1988.

Kay, S. M. and S. L. Marple, Spectrum Analysis-A Modern Perspective *Proc. IEEE*, **69**, 1981.

Kelley, M. C., B. G. Fejer and C. A. Gonzales, An explanation for anomalous ionospheric electric fields associated with a northward turning of the interplanetary magnetic field, *Geophys. Res. Lett.*, **6**, 301, 1979.

Klobuchar, J. A., D. N. Anderson and P. H. Doherty, Model studies of the latitudinal extent of the equatorial anomaly during equinoctial conditions, *Radio Science*, **26**, 1025, 1991.

Maruyama, T. and N. Matuura, Longitudinal variability of annual changes in

activity of equatorial spread-F and plasma bubbles, *J. Geophys. Res.*, **89**, 10903, 1984.

Mendillo, M., M. D. Papagiannis and J. A. Klobuchar, Average behavior of the mid-latitude *F*-region parameters, N_T, N_{max} and τ during magnetic storms, *J. Geophys. Res.*, **77**, 4891, 1972.

Mendillo, M., X. Q. He, and H. Rishbeth, How the effects of winds and electric fields in F_2-layer storms vary with latitude and longitude: a theoretical study, *Planet. Space Sci.*, *40*, 595, 1992a.

Mendillo, M., J. Baumgardner, X.-Q. Pi, P. J. Sultan and R. T. Tsunoda, Onset conditions for equatorial spread-F, *J. Geophys. Res.*, **97**, 13865, 1992b.

Oppenheim, A. V. and R. W. Schafer, *Discrete-time Signal Processing*, Prentice Hall, Englewood Cliffs, New Jersey, 1989.

Parish, H.F., Quasi two-day oscillations in the low latitude ionosphere, *Eos*, Supplement, April 19, 1994.

Pi, X., M. Mendillo, M. W. Fox, and D. N. Anderson, Diurnal double maxima patterns in the *F* region ionosphere: Substorm-related aspects, *J. Geophys. Res.*, **98**, 13677, 1993.

Preble, A. J., D. N. Anderson, B. G. Fejer and P. H. Doherty, Comparison between calculated and observed F-region electron density profiles at Jicamarca, Peru, *Radio Science*, In press, 1994.

Prölss, G. W., L. H. Brace, H. G. Mayr, G. R. Carignan, T. L. Killeen and J. A. Klobuchar, Ionospheric storm effects at subauroral latitudes: A case study, *J. Geophys. Res.*, **96**, 1275, 1991.

Prölss, G. W., Common origin of positive ionospheric storms at middle latitudes and the geomagnetic activity effect at low latitudes, *J. Geophys. Res.*, **98**, 5981, 1993.

Reddy, C. A., S. Fukao, T. Takami, M. Yamamoto, T. Tsuda, T. Nakamura and

S Kato, A MU radar-based study of mid-latitude F-region response to a geomagnetic disturbance, *J. Geophys. Res.*, **95**, 21077, 1990.

Rishbeth, H., F region storms and thermospheric circulation, *J. Atmos. Terr. Phys.*, **37**, 1055, 1975.

Rishbeth, H., T. J. Fuller-Rowell and A. S. Rodger, F-layer storms and thermospheric composition, *Physica Scripta*, **36**, 327, 1978.

Spiro, R. W., R. A. Wolf, and B. G. Fejer, Penetration of high-latitude-electric-field effects to low latitudes during SUNDIAL 1984, *Ann. Geophysicae*, **6**, 39, 1988.

Titheridge, J. E. and M. J. Buonsanto, A comparison of northern and southern hemisphere TEC storm behavior, *J. Atmos. Terr. Phys.*, **50**, 763, 1988.

Tobiska, W. K., Recent extreme ultrviolet irradiance observations and modeling: A review, *J. Geophys. Res.*, **98**, 18879, 1993.

Tsunoda, R. T., Control of the seasonal and longitudinal occurrence of equatorial scintillations by the longitudinal gradient in the integrated E-region Pederson conductivity. *J. Geophys. Res.*, **90**, 447, 1985.

Vasyliunas, V. M., The interrelationship of magnetospheric processes, **Earth's Magnetospheric Processes**, (B. M. McCormac, ed.), p. 29, Reidel, Boston Massachusetts, 1972.

Wrenn, G. L. and A. S. Rodger, Geomagtnetic modification of the mid-latitude ionsosphere: Toward a strategy for the improved forecasting of foF2, *Radio Science*, **24**, 99, 1989.

Figure 1.

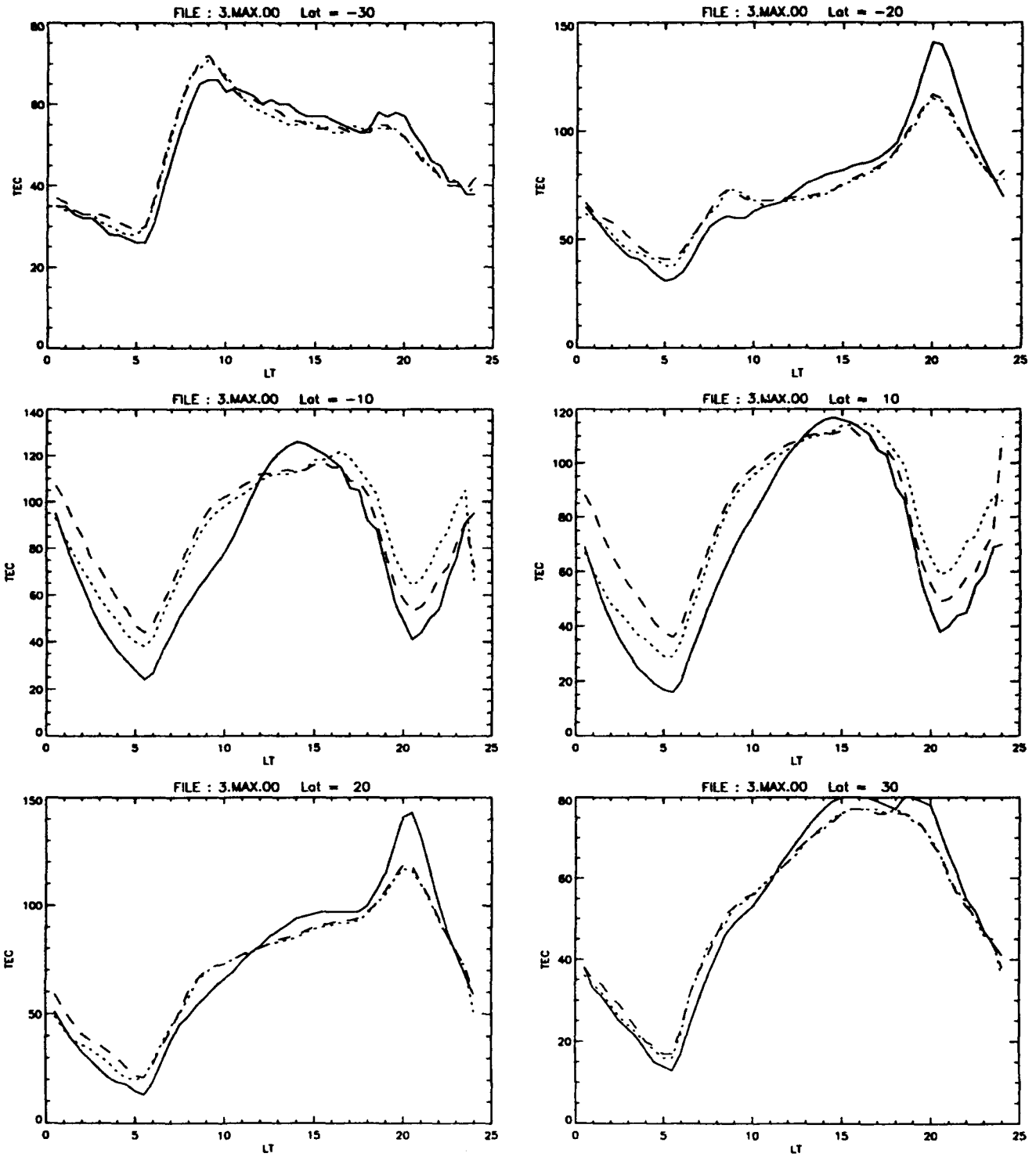
FILE : 3.MAX.00 Lat = -30
FILE : 3.MAX.00 Lat = -20
FILE : 3.MAX.00 Lat = -10
FILE : 3.MAX.00 Lat = 10
FILE : 3.MAX.00 Lat = 20
FILE : 3.MAX.00 Lat = 30
TEC
LT

Figure 2.

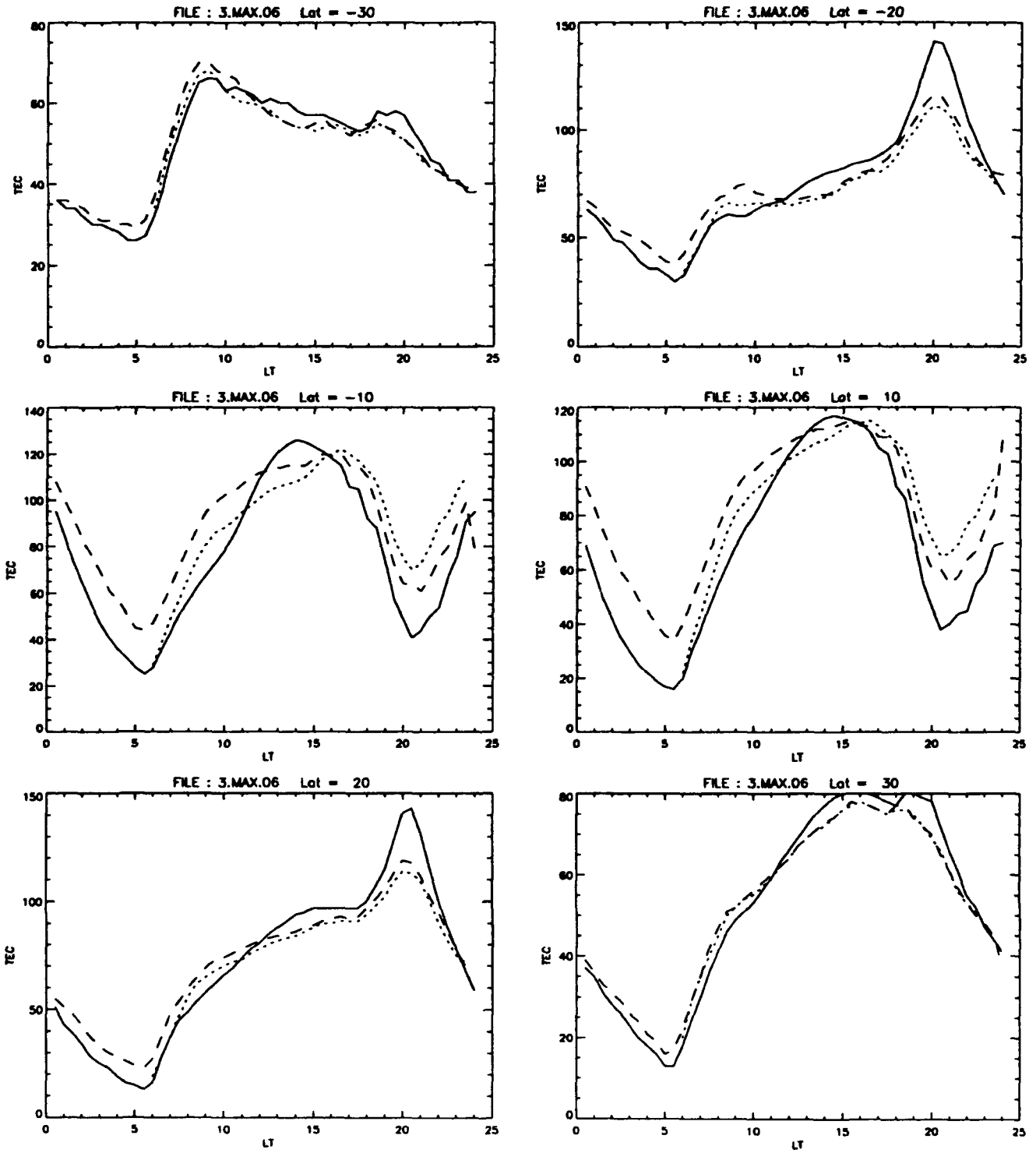
FILE : 3.MAX.06 Lat = -30
FILE : 3.MAX.06 Lat = -20
FILE : 3.MAX.06 Lat = -10
FILE : 3.MAX.06 Lat = 10
FILE : 3.MAX.06 Lat = 20
FILE : 3.MAX.06 Lat = 30
TEC
LT

Figure 3.

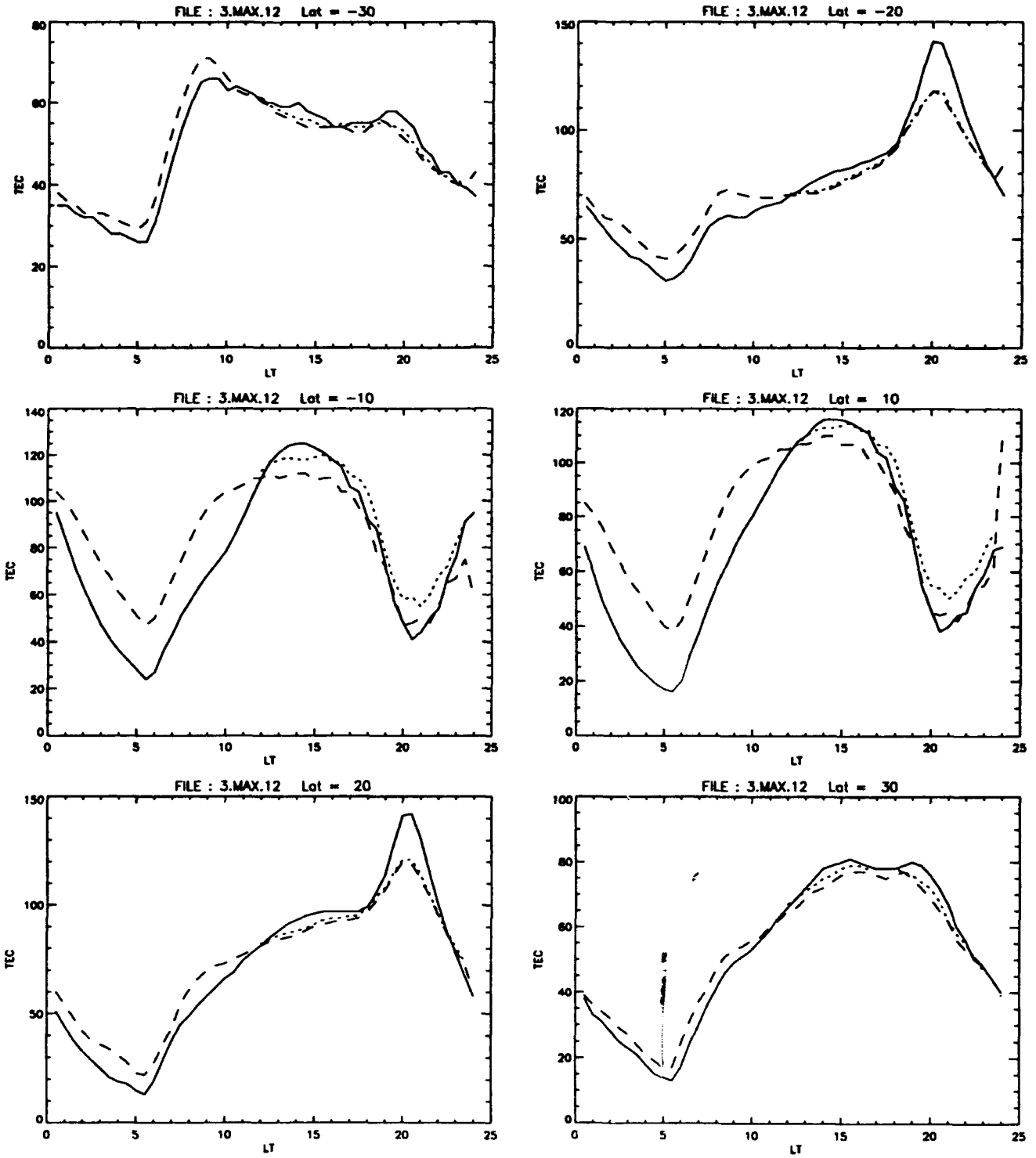
FILE : 3.MAX.12 Lat = -30
FILE : 3.MAX.12 Lat = -20
FILE : 3.MAX.12 Lat = -10
FILE : 3.MAX.12 Lat = 10
FILE : 3.MAX.12 Lat = 20
FILE : 3.MAX.12 Lat = 30
TEC
LT

Figure 4.

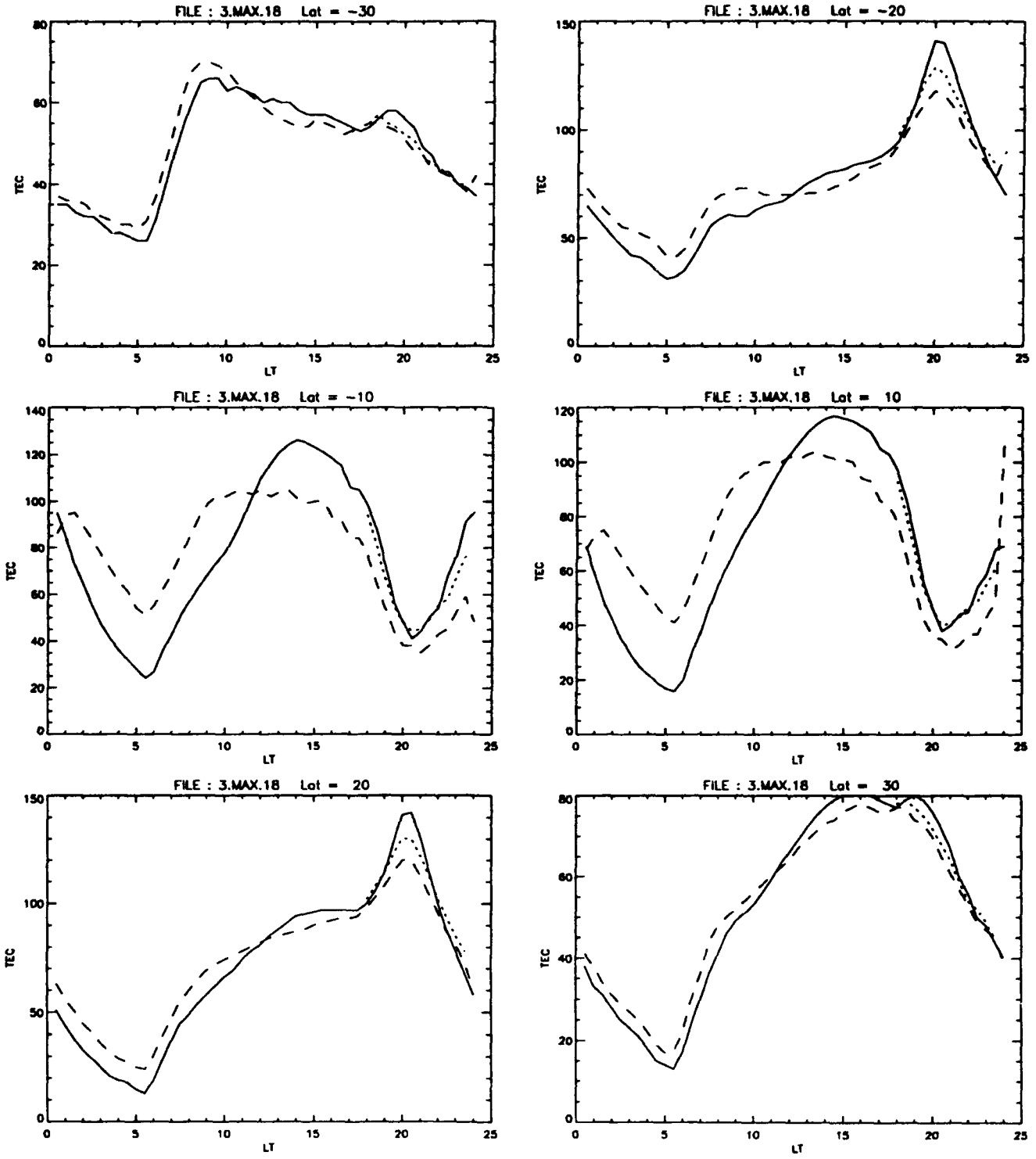
FILE : 3.MAX.18 Lat = -30
FILE : 3.MAX.18 Lat = -20
FILE : 3.MAX.18 Lat = -10
FILE : 3.MAX.18 Lat = 10
FILE : 3.MAX.18 Lat = 20
FILE : 3.MAX.18 Lat = 30
TEC
LT

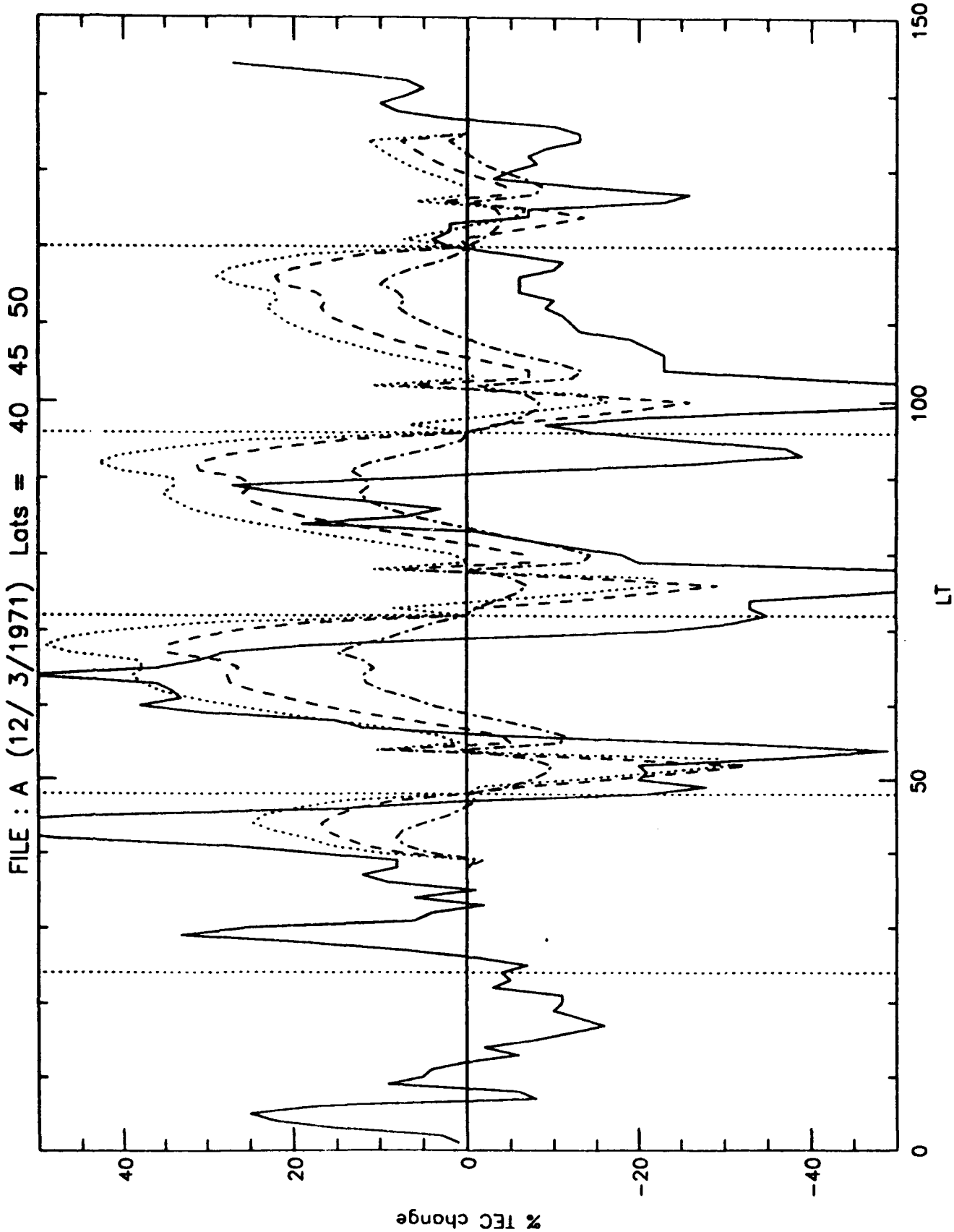
FILE : A (12/ 3/1971) Lats = 40 45 50
% TEC change
40
20
0
-20
-40
0
50
100
150
LT

Figure 5.

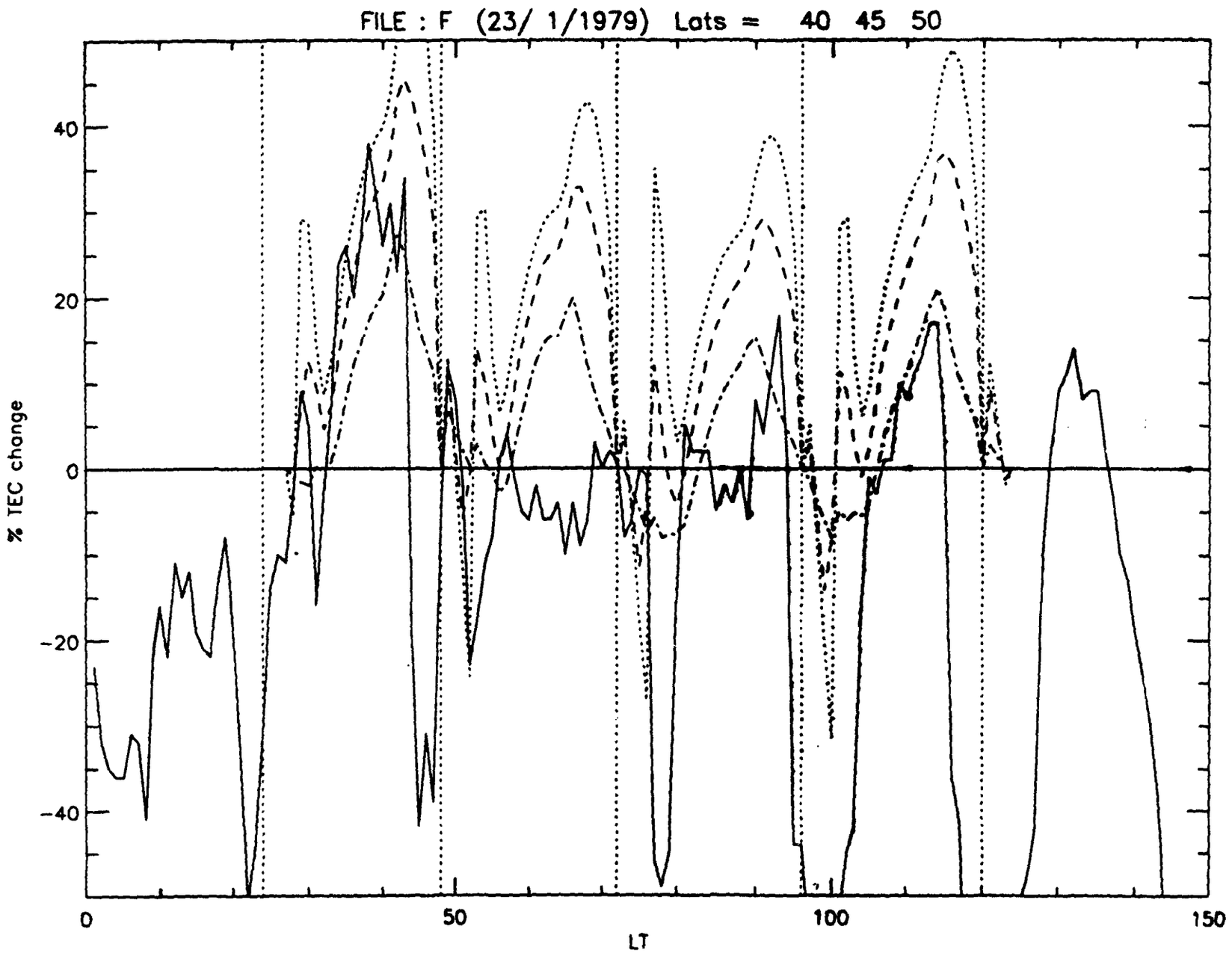
FILE : F (23/ 1/1979) Lats = 40 45 50
% TEC change
40
20
0
-20
-40
0
50
100
150
LT

Figure 6.

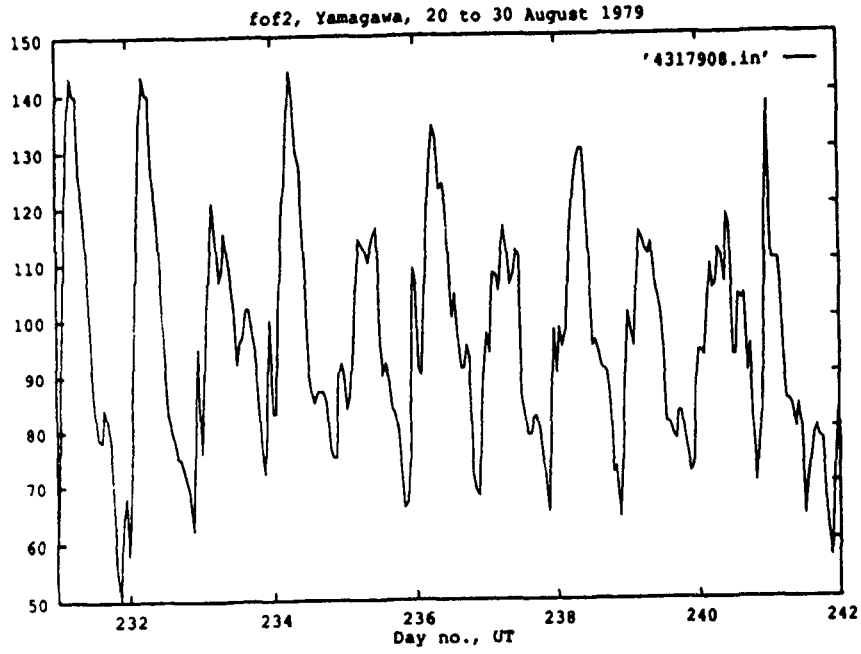

foF2, Townsville, 20 to 30 August 1979

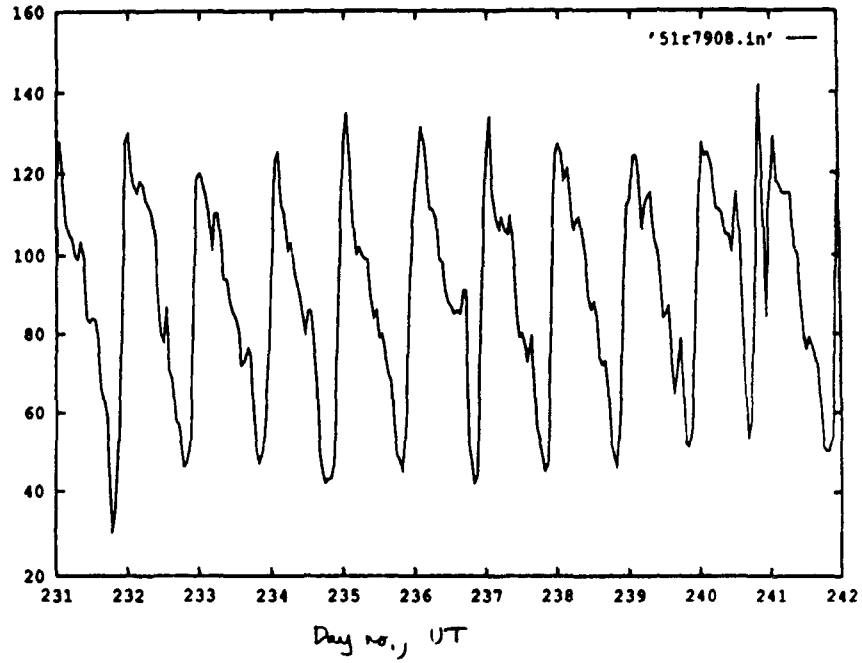

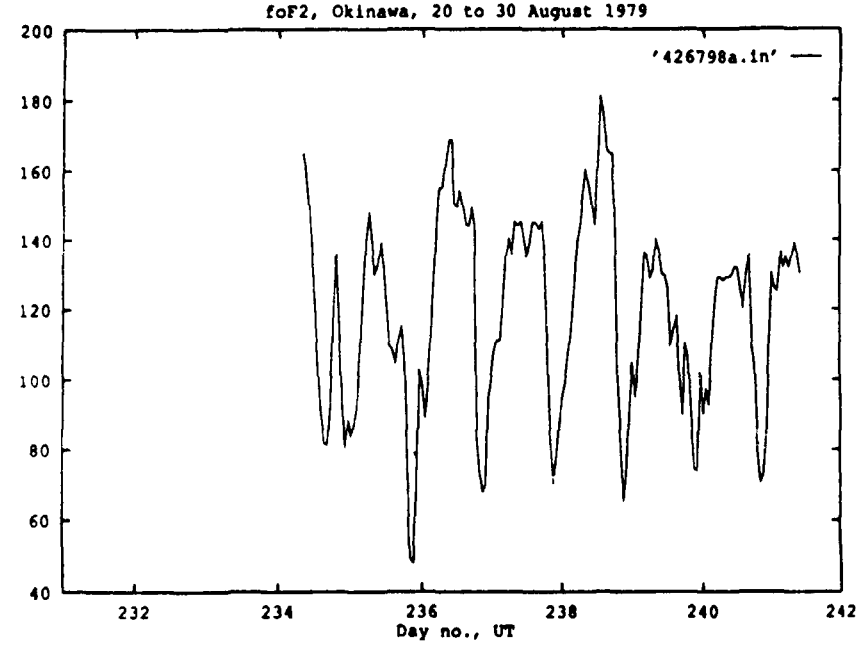

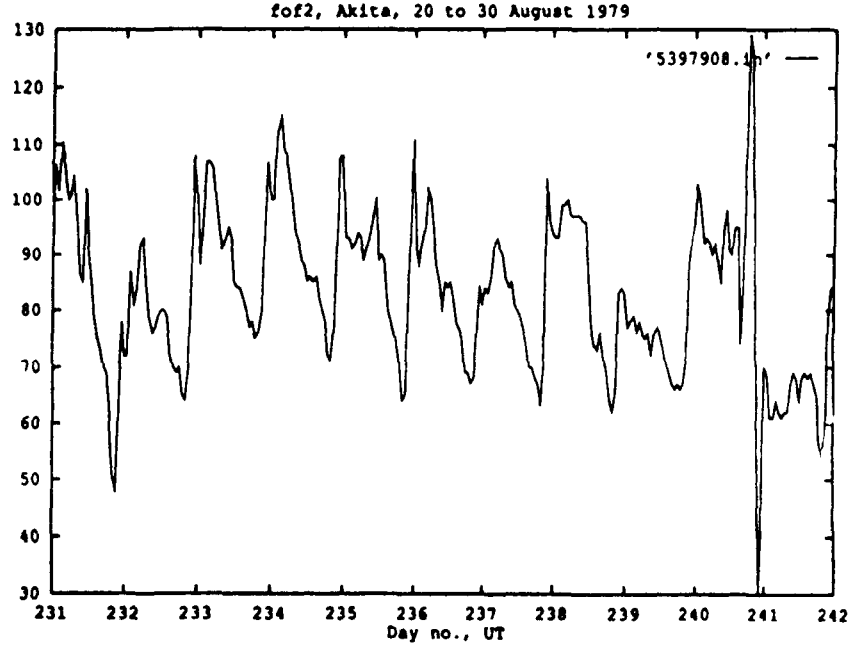

Figure 7.

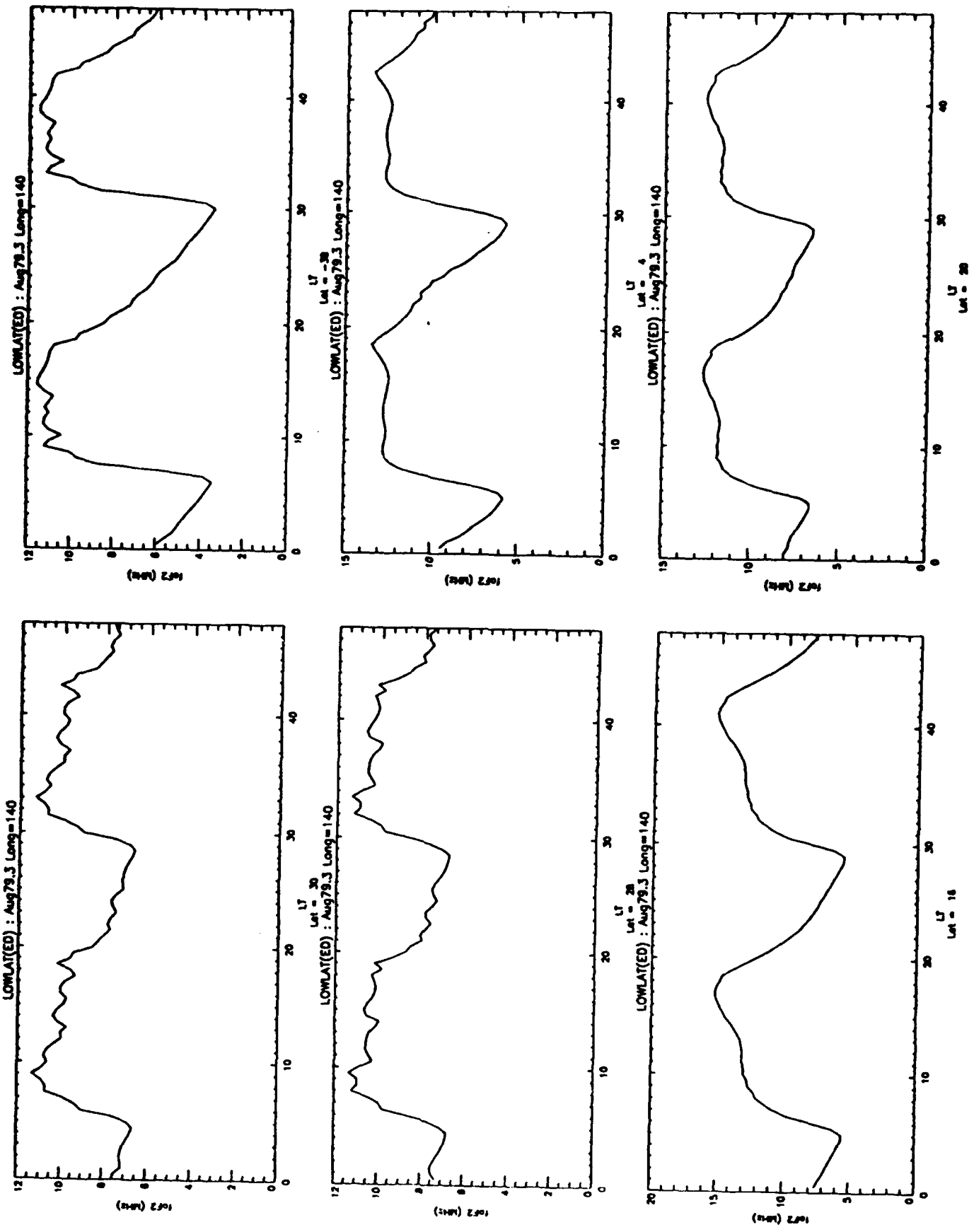
LOWLAT(ED) : Aug79.3 Long=140
LOWLAT(ED) : Aug79.3 Long=140
LOWLAT(ED) : Aug79.3 Long=140
LOWLAT(ED) : Aug79.3 Long=140
LOWLAT(ED) : Aug79.3 Long=140
LOWLAT(ED) : Aug79.3 Long=140

Figure 8.

Figure 9.

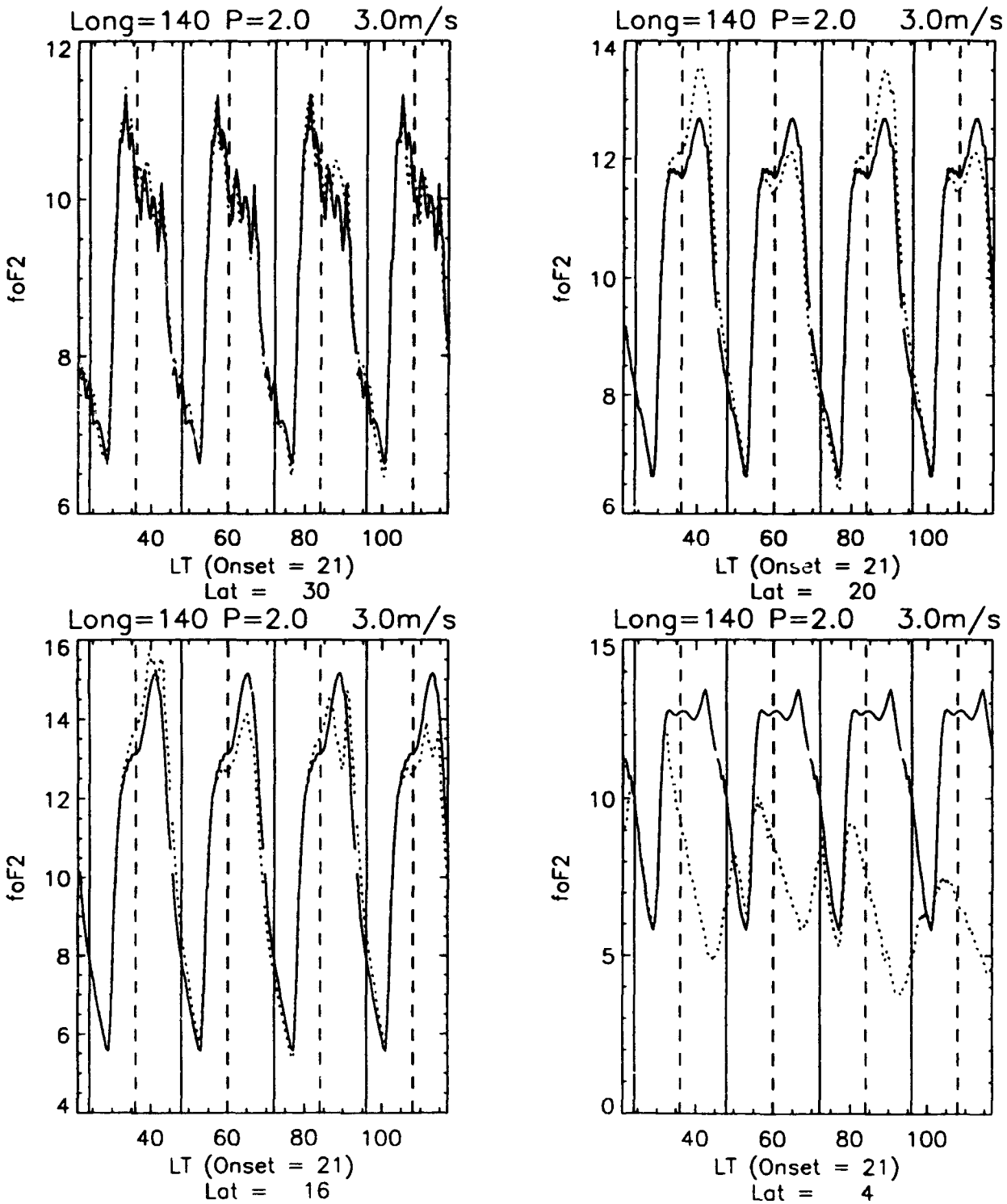
Long=140 P=2.0 3.0m/s
foF2
LT (Onset = 21)
Lat = 30
Long=140 P=2.0 3.0m/s
foF2
LT (Onset = 21)
Lat = 20
Long=140 P=2.0 3.0m/s
foF2
LT (Onset = 21)
Lat = 16
Long=140 P=2.0 3.0m/s
foF2
LT (Onset = 21)
Lat = 4

Figure 10.

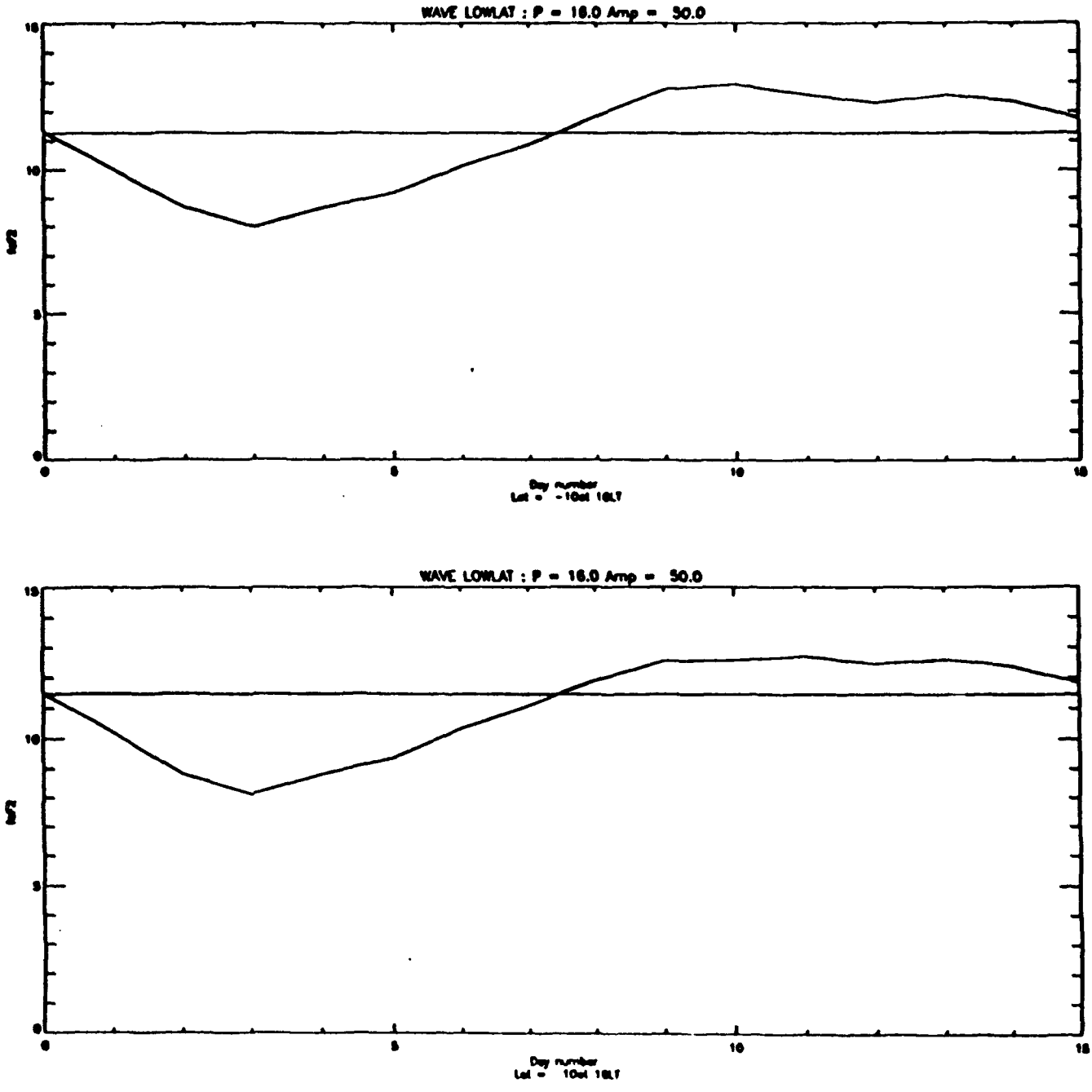
WAVE LOWLAT : P = 16.0 Amp = 50.0
Day number
WAVE LOWLAT : P = 16.0 Amp = 50.0
Day number

Figure 11.

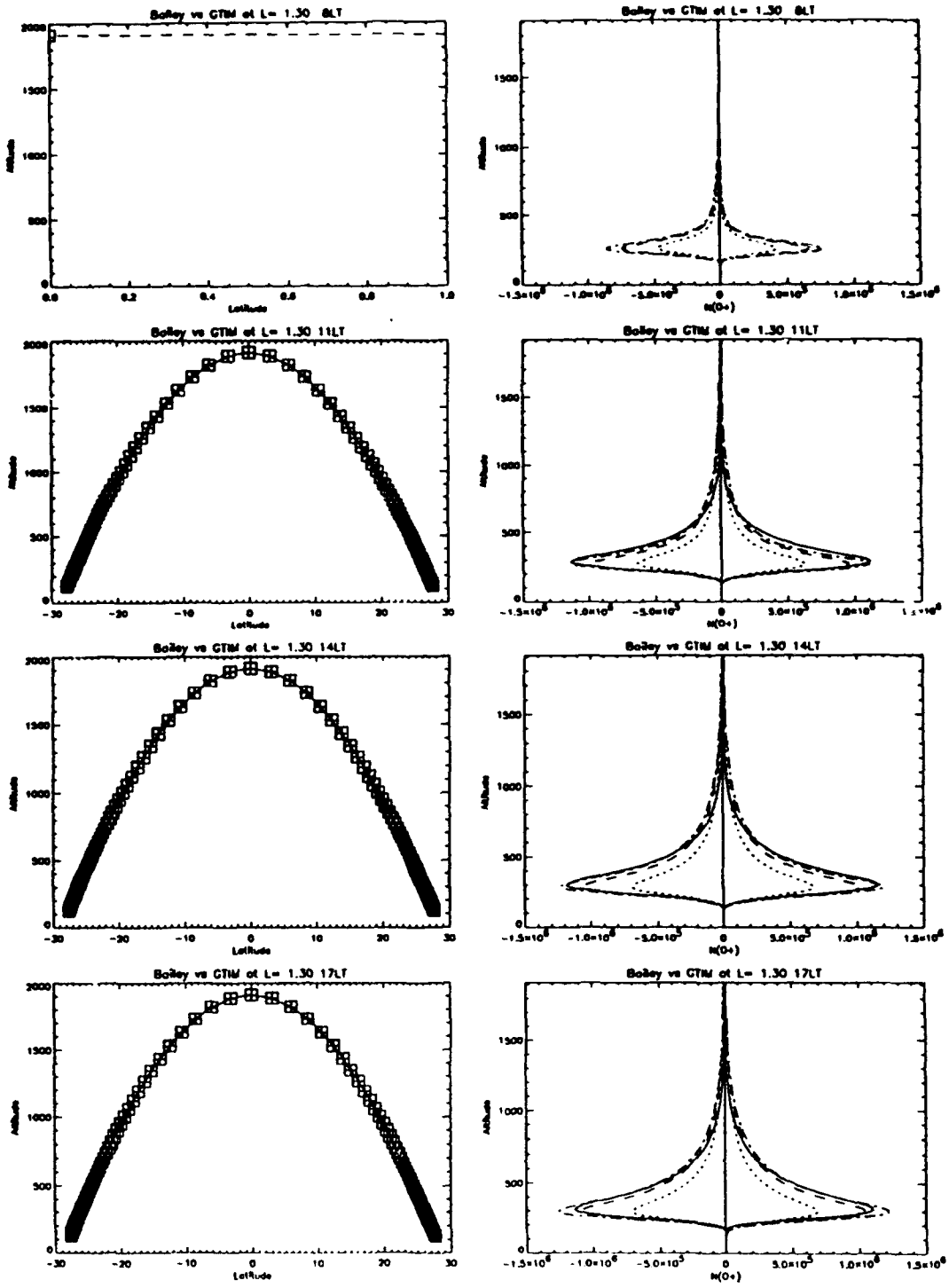
Bailey vs GTIM at L= 1.30 8LT
Bailey vs GTIM at L= 1.30 11LT
Bailey vs GTIM at L= 1.30 14LT
Bailey vs GTIM at L= 1.30 17LT
Altitude
Latitude
N(O+)

Figure 12.

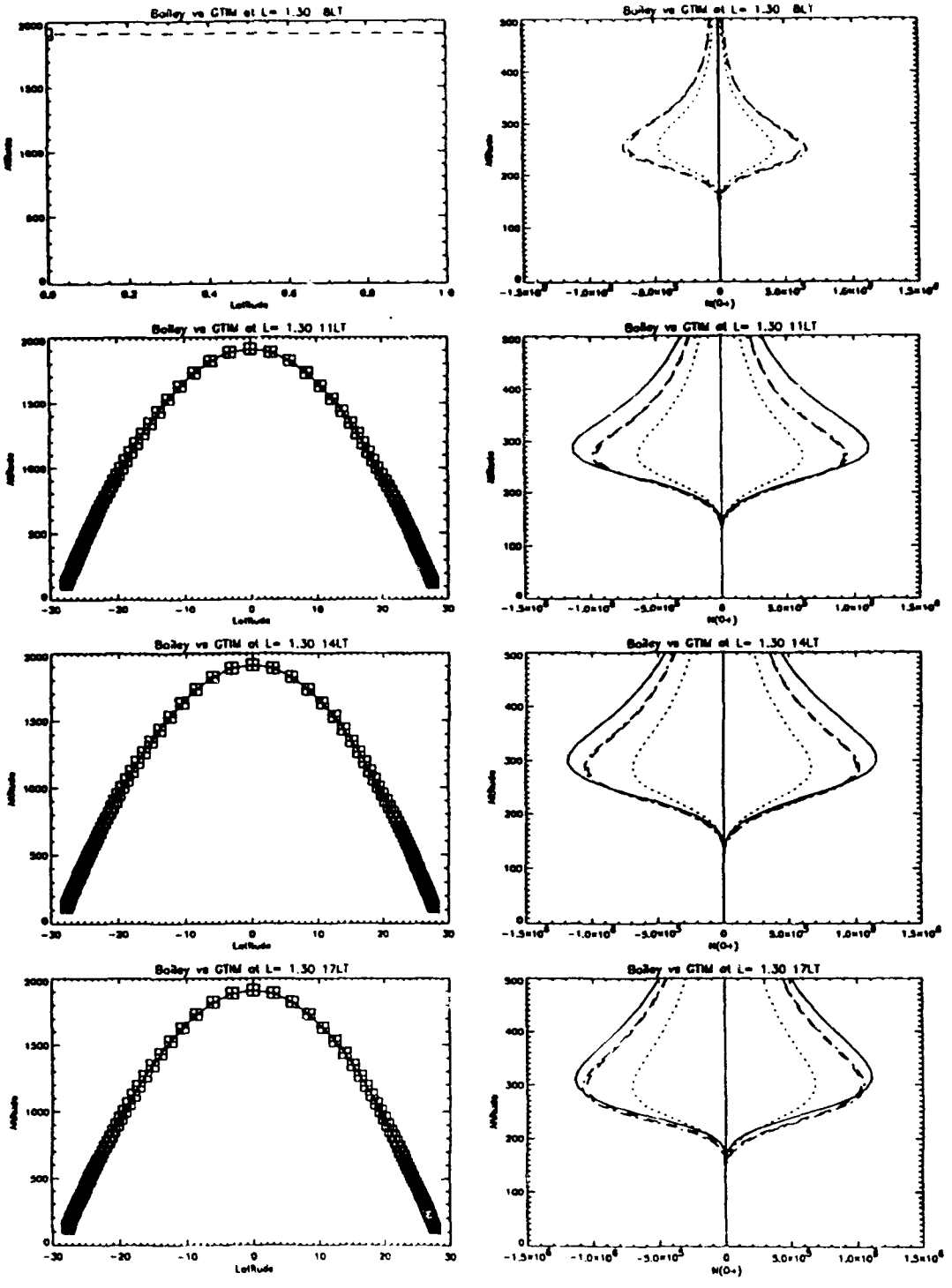
Bailey vs GTIM at L= 1.30 8LT
Bailey vs GTIM at L= 1.30 11LT
Bailey vs GTIM at L= 1.30 14LT
Bailey vs GTIM at L= 1.30 17LT
Altitude
Latitude
N(O+)

Figure 13.

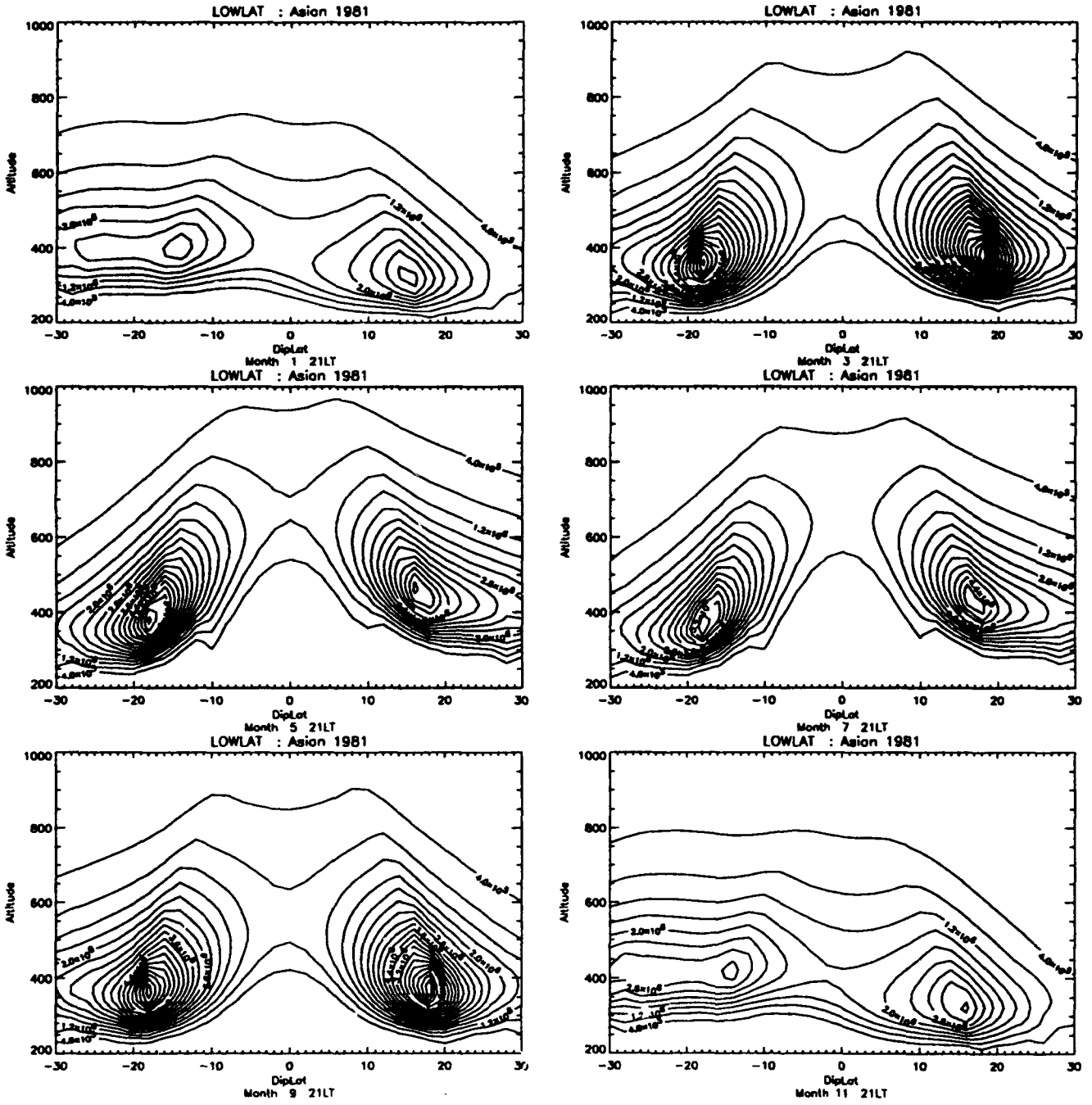
LOWLAT : Asian 1981
Altitude
DipLat
Month 1 21LT
LOWLAT : Asian 1981
Altitude
DipLat
Month 3 21LT
LOWLAT : Asian 1981
Altitude
DipLat
Month 5 21LT
LOWLAT : Asian 1981
Altitude
DipLat
Month 7 21LT
LOWLAT : Asian 1981
Altitude
DipLat
Month 9 21LT
LOWLAT : Asian 1981
Altitude
DipLat
Month 11 21LT

Figure 14.

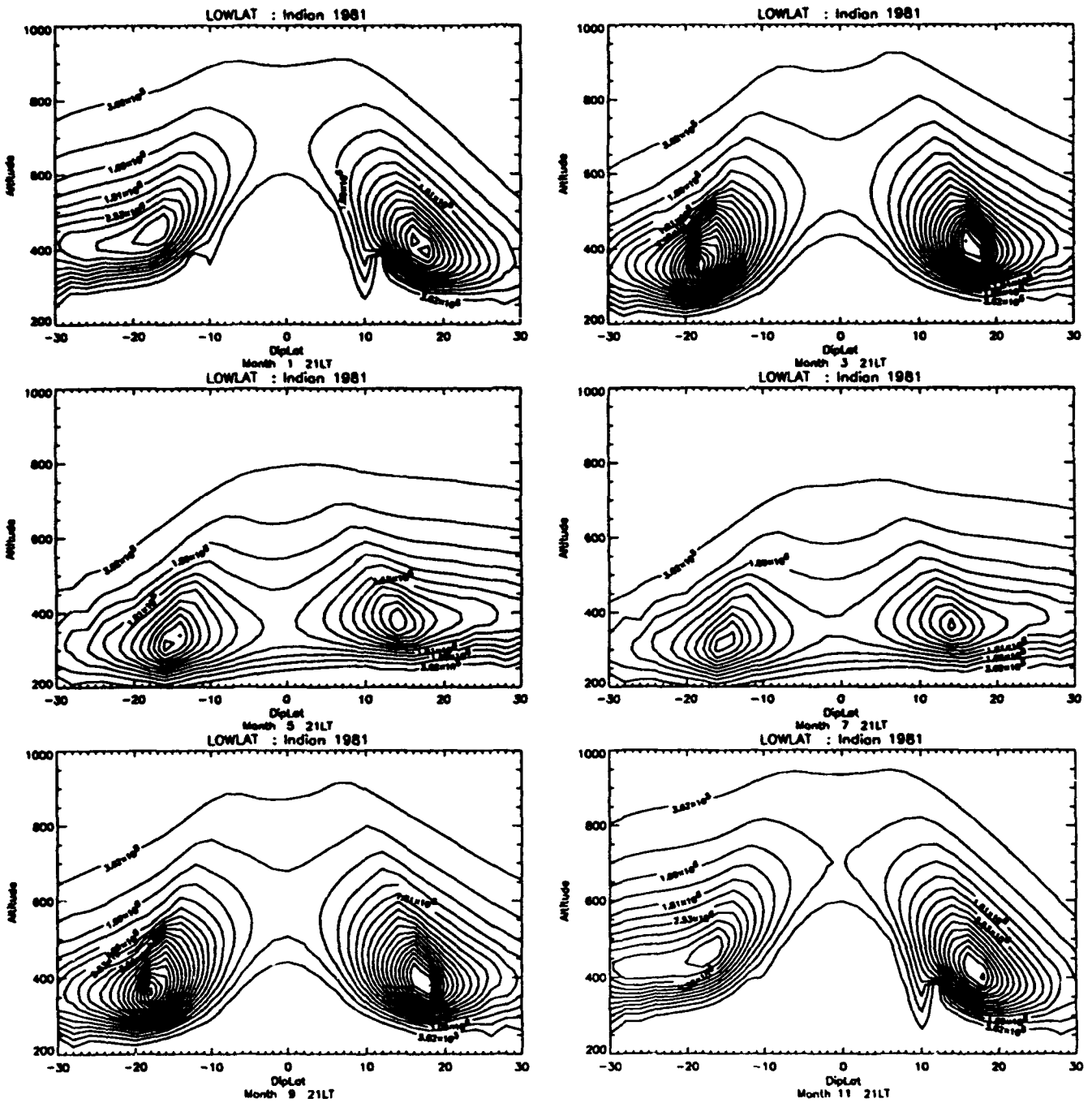
LOWLAT : Indian 1981
Altitude
DipLat
Month 1 21LT
LOWLAT : Indian 1981
Altitude
DipLat
Month 3 21LT
LOWLAT : Indian 1981
Altitude
DipLat
Month 5 21LT
LOWLAT : Indian 1981
Altitude
DipLat
Month 7 21LT
LOWLAT : Indian 1981
Altitude
DipLat
Month 9 21LT
LOWLAT : Indian 1981
Altitude
DipLat
Month 11 21LT

Figure 15.

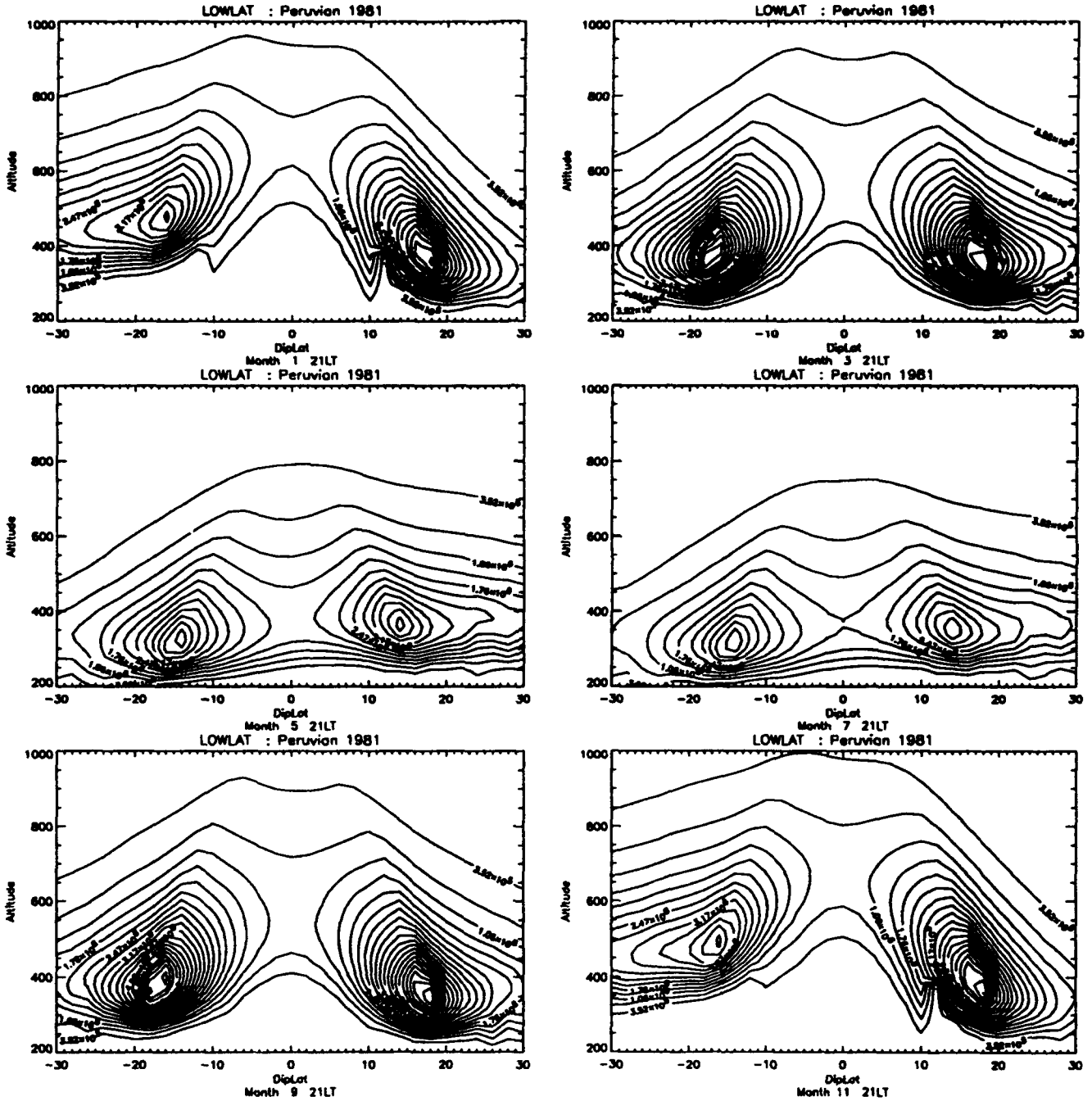
LOWLAT : Peruvian 1981
Altitude
DipLat
Month 1 21LT
LOWLAT : Peruvian 1981
Altitude
DipLat
Month 3 21LT
LOWLAT : Peruvian 1981
Altitude
DipLat
Month 5 21LT
LOWLAT : Peruvian 1981
Altitude
DipLat
Month 7 21LT
LOWLAT : Peruvian 1981
Altitude
DipLat
Month 9 21LT
LOWLAT : Peruvian 1981
Altitude
DipLat
Month 11 21LT

Figure 16.

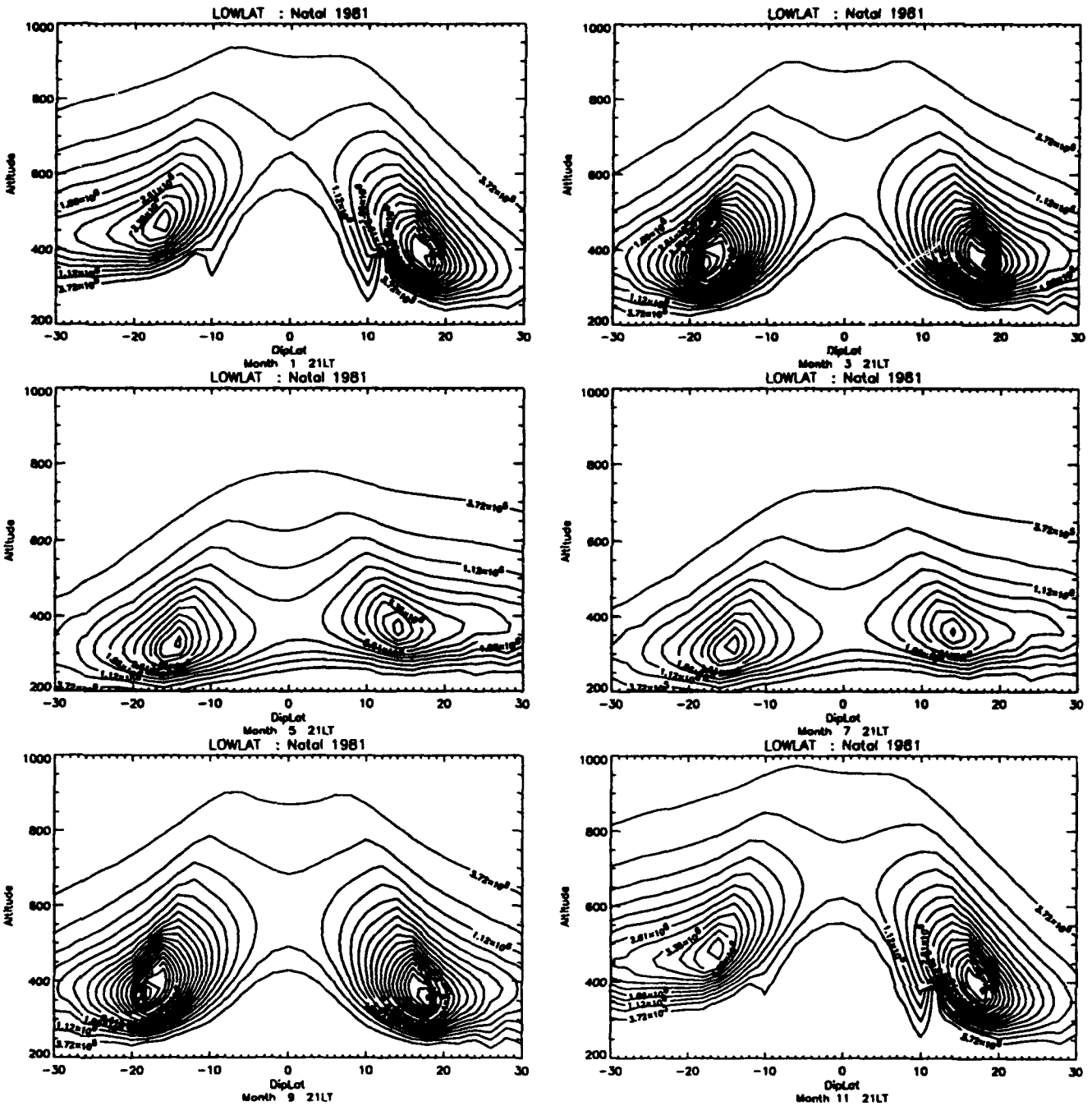
LOWLAT : Natal 1981
Altitude
DipLat
Month 1 21LT
LOWLAT : Natal 1981
Altitude
DipLat
Month 3 21LT
LOWLAT : Natal 1981
Altitude
DipLat
Month 5 21LT
LOWLAT : Natal 1981
Altitude
DipLat
Month 7 21LT
LOWLAT : Natal 1981
Altitude
DipLat
Month 9 21LT
LOWLAT : Natal 1981
Altitude
DipLat
Month 11 21LT

Figure 17.

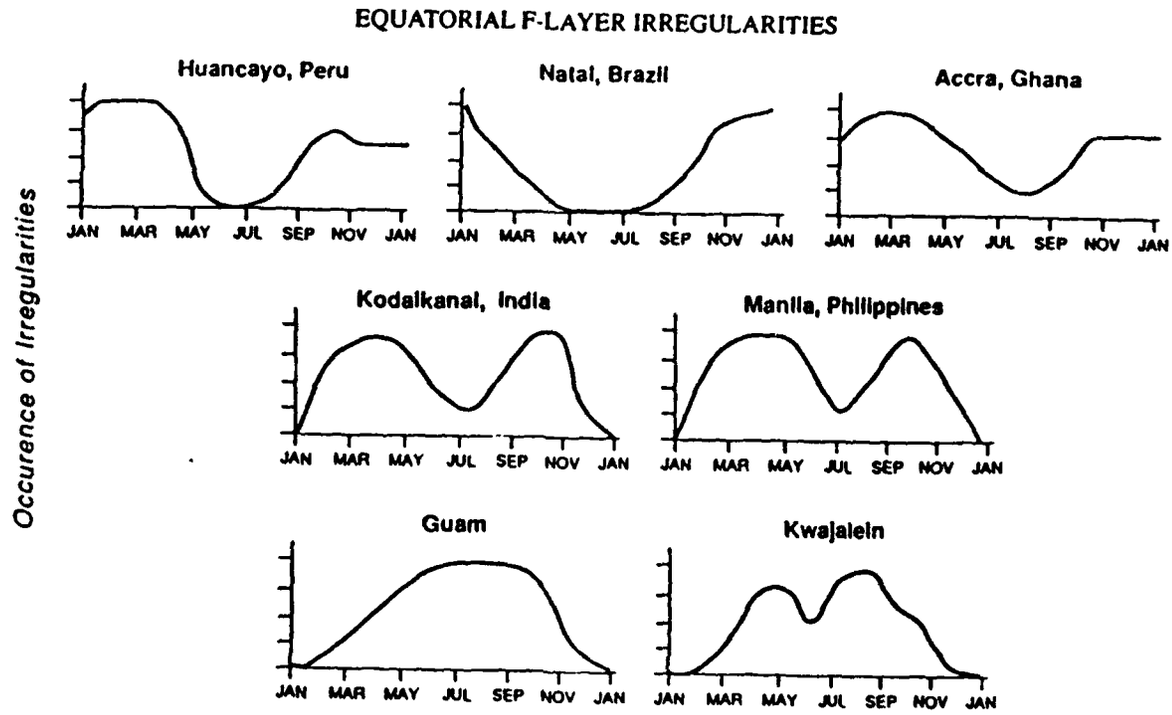

Using the scintillation data as indicating the F-layer irregularities from all types of layers but predominantly from exxtended layers, it is possible to develop a sense of the morphology. We have attempted to do so in this figure. There are caveats however. The maximum amplitude of the excursion shown for each area is arbitrarily shown as 4 units; it is possible that some areas have both increased intensity and increased occurrence relative to other areas. In addition there is no distinction made between high and low solar flux years. The pattern attempts to merge the two occurrence patterns from the data set but there may well be differences.

Figure 18.

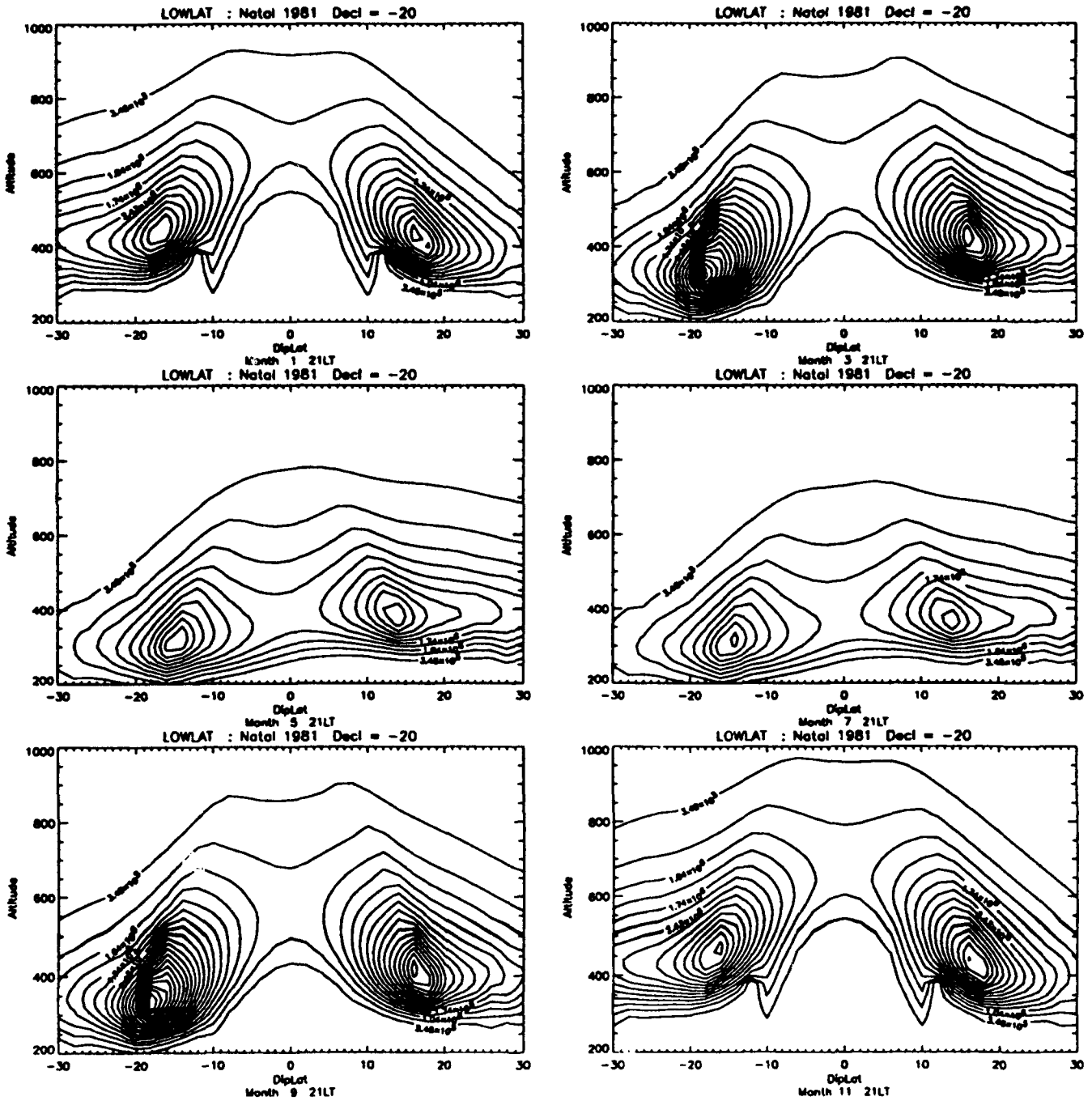
LOWLAT : Natal 1981 Decl = -20
Altitude
DipLat
Month 1 21LT
LOWLAT : Natal 1981 Decl = -20
Altitude
DipLat
Month 3 21LT
LOWLAT : Natal 1981 Decl = -20
Altitude
DipLat
Month 5 21LT
LOWLAT : Natal 1981 Decl = -20
Altitude
DipLat
Month 7 21LT
LOWLAT : Natal 1981 Decl = -20
Altitude
DipLat
Month 9 21LT
LOWLAT : Natal 1981 Decl = -20
Altitude
DipLat
Month 11 21LT

Figure 19.

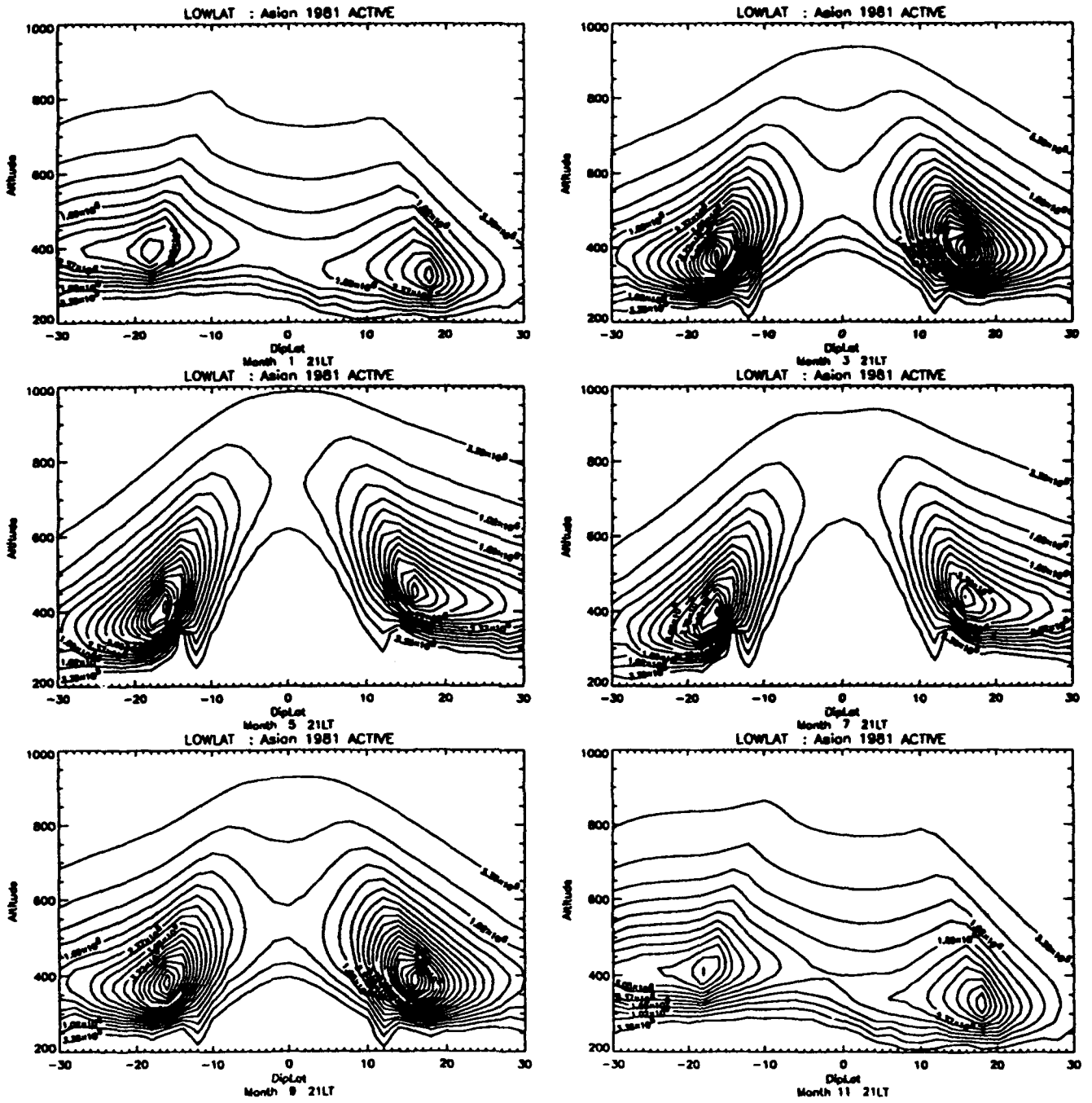
LOWLAT : Asian 1981 ACTIVE
Altitude
DipLat
Month 1 21LT
LOWLAT : Asian 1981 ACTIVE
Altitude
DipLat
Month 3 21LT
LOWLAT : Asian 1981 ACTIVE
Altitude
DipLat
Month 5 21LT
LOWLAT : Asian 1981 ACTIVE
Altitude
DipLat
Month 7 21LT
LOWLAT : Asian 1981 ACTIVE
Altitude
DipLat
Month 9 21LT
LOWLAT : Asian 1981 ACTIVE
Altitude
DipLat
Month 11 21LT

Figure 20.

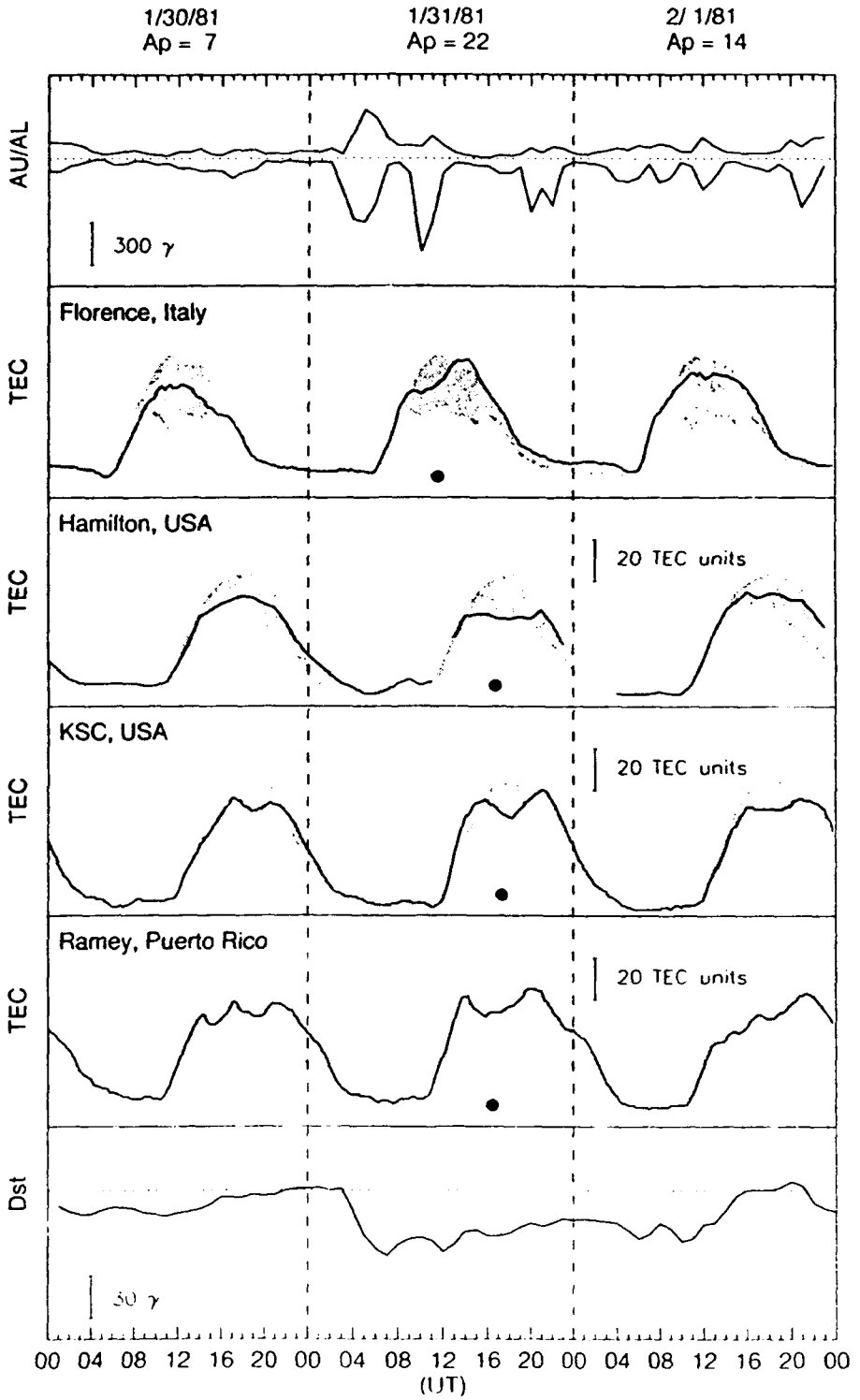
1/30/81
Ap = 7
1/31/81
Ap = 22
2/ 1/81
Ap = 14
AU/AL
300 γ
Florence, Italy
TEC
Hamilton, USA
TEC
20 TEC units
KSC, USA
TEC
20 TEC units
Ramey, Puerto Rico
TEC
20 TEC units
Dst
50 γ
00 04 08 12 16 20 00 04 08 12 16 20 00 04 08 12 16 20 00
(UT)

Figure 21.

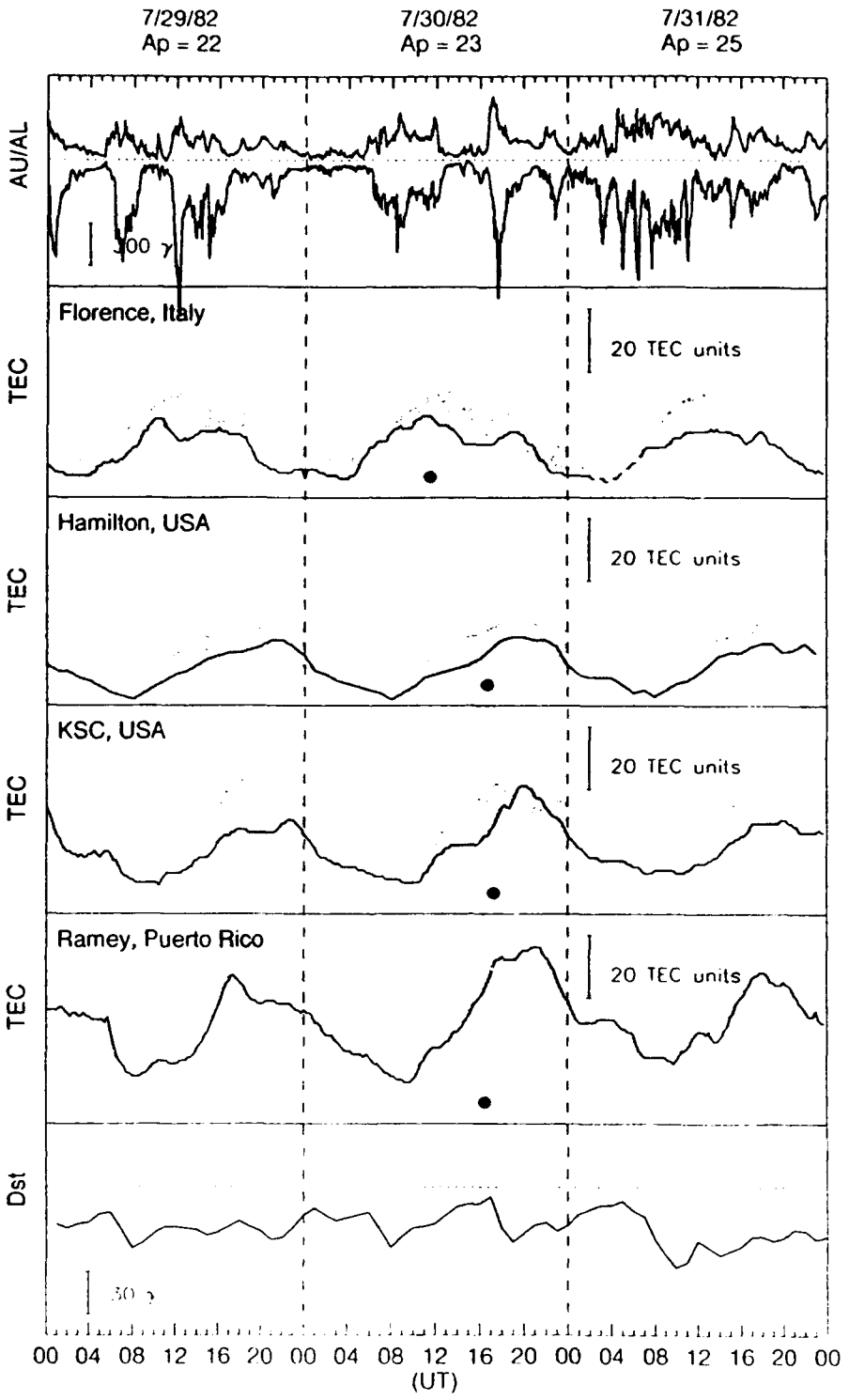
7/29/82
Ap = 22
7/30/82
Ap = 23
7/31/82
Ap = 25
AU/AL
300 γ
Florence, Italy
20 TEC units
TEC
Hamilton, USA
20 TEC units
TEC
KSC, USA
20 TEC units
TEC
Ramey, Puerto Rico
20 TEC units
TEC
Dst
00 04 08 12 16 20 00 04 08 12 16 20 00 04 08 12 16 20 00
(UT)

Figure 22.

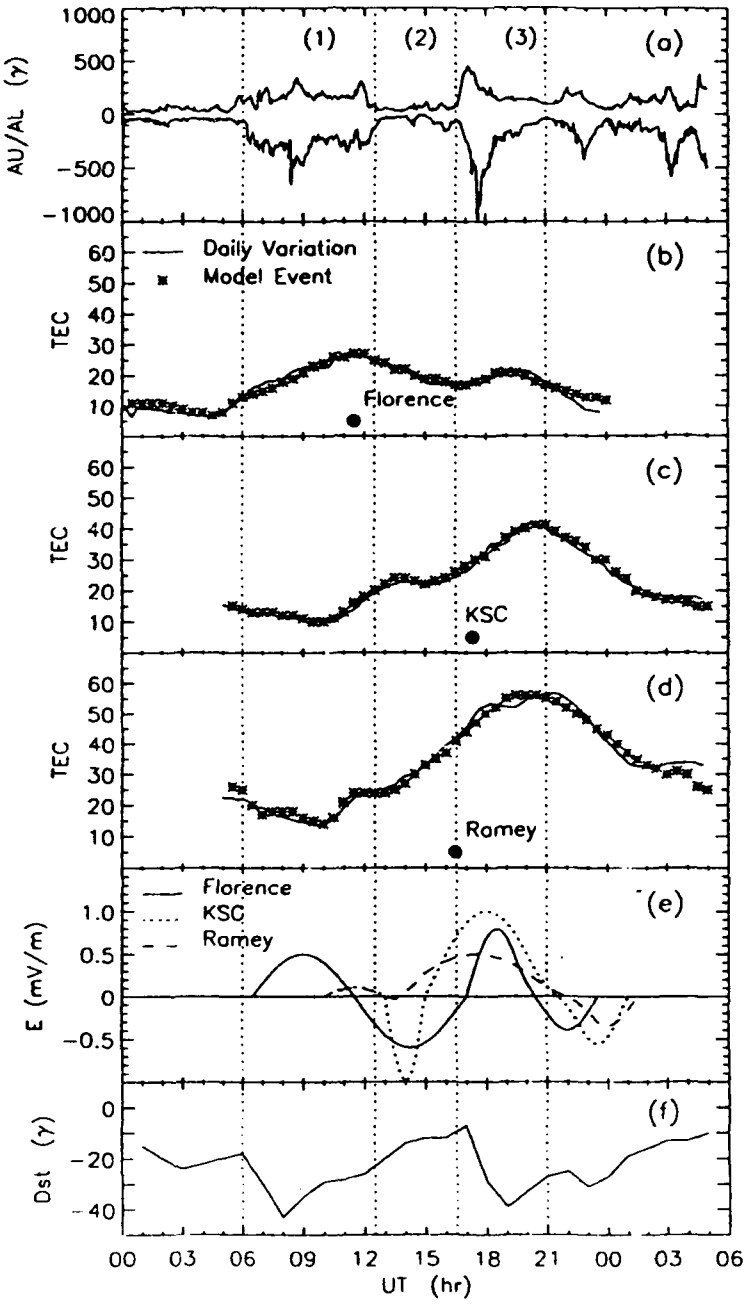

July 30, 1982.

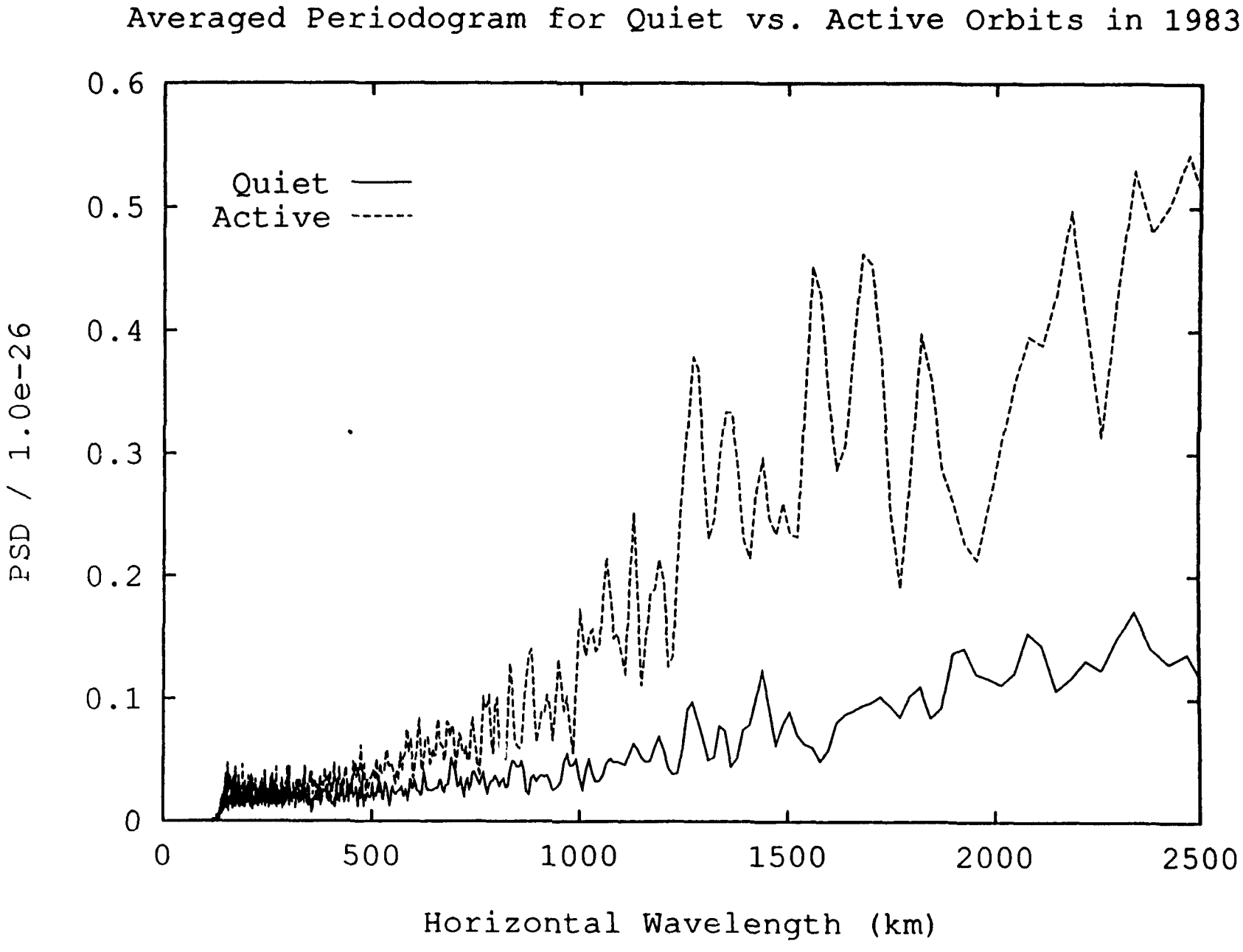
Averaged Periodogram for Quiet vs. Active Orbits in 1983
Quiet
Active
PSD / 1.0e-26
0.6
0.5
0.4
0.3
0.2
0.1
0
0
500
1000
1500
2000
2500
Horizontal Wavelength (km)

Figure 23.

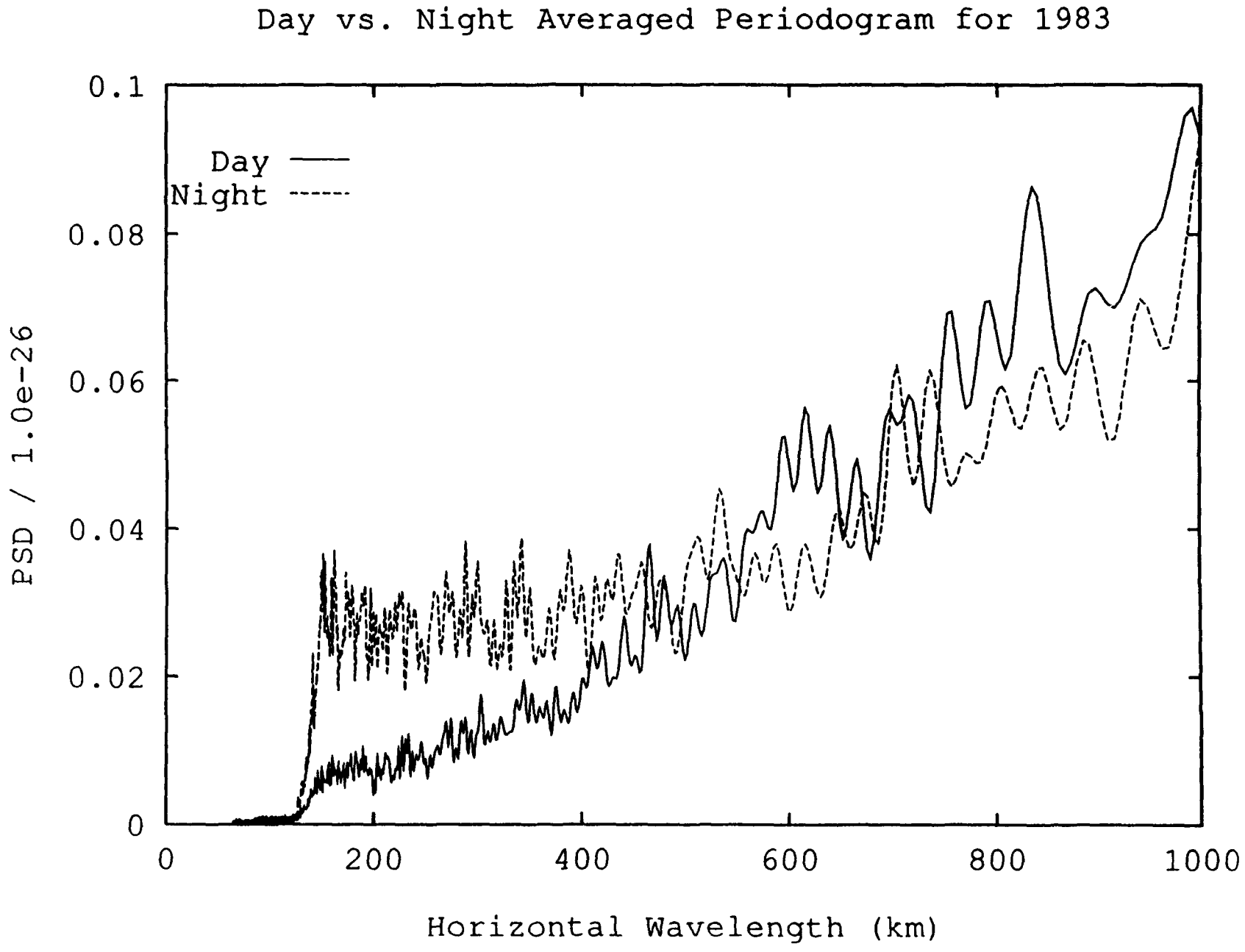
Day vs. Night Averaged Periodogram for 1983
Day
Night
PSD / 1.0e-26
0.1
0.08
0.06
0.04
0.02
0
0
200
400
600
800
1000
Horizontal Wavelength (km)

Figure 24.

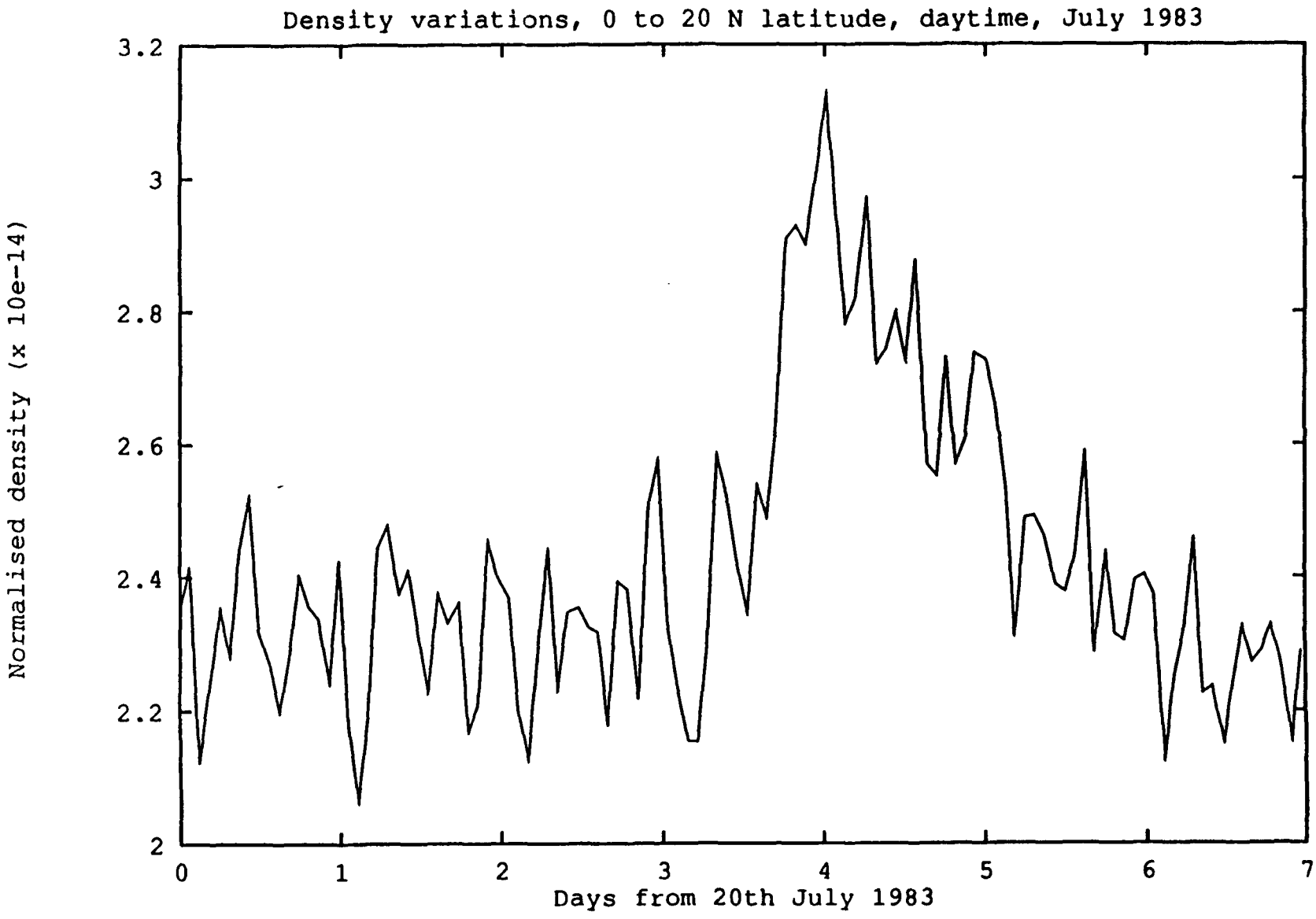
Density variations, 0 to 20 N latitude, daytime, July 1983
Normalised density (x 10e-14)
3.2
3
2.8
2.6
2.4
2.2
2
0
1
2
3
4
5
6
7
Days from 20th July 1983

Figure 25.